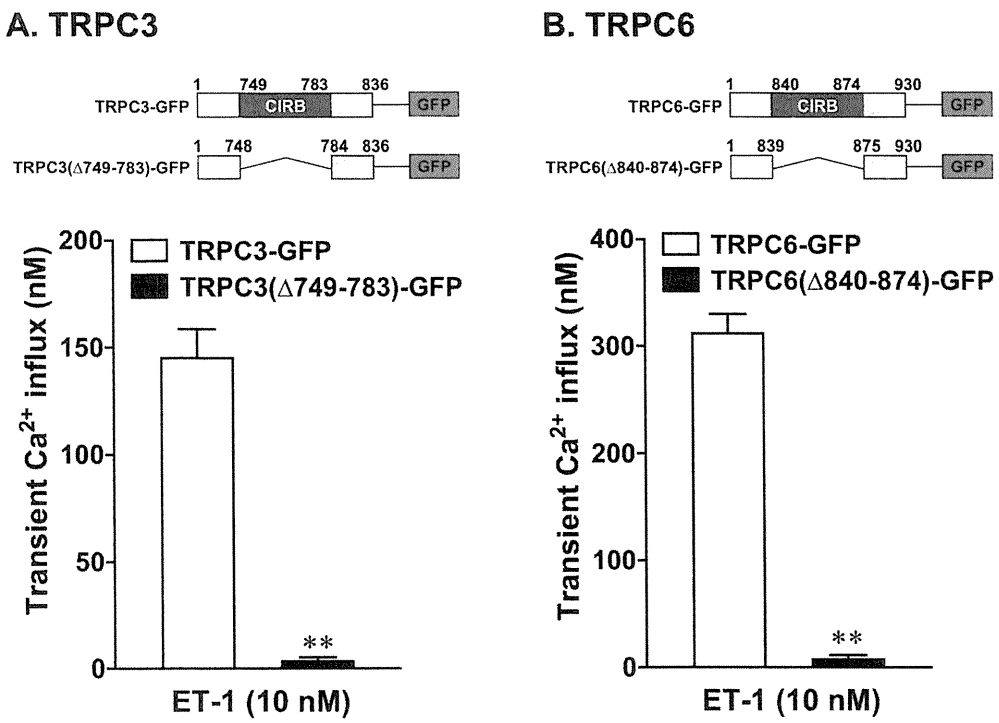

Fig. 4. Significance of CIRB domain at the C terminus of TRPC3 (A) and TRPC6 (B) in channel activity. Influence of deletion of CIRB domain in ROCE induced by 10 nM ET-1 was estimated by $[Ca^{2+}]_i$ measurement. Data are presented as the mean ± S.E.M. of the results obtained from 4–6 experiments. $^{**}P < 0.01$ vs. wild type (TRPC3-GFP or TRPC6-GFP).

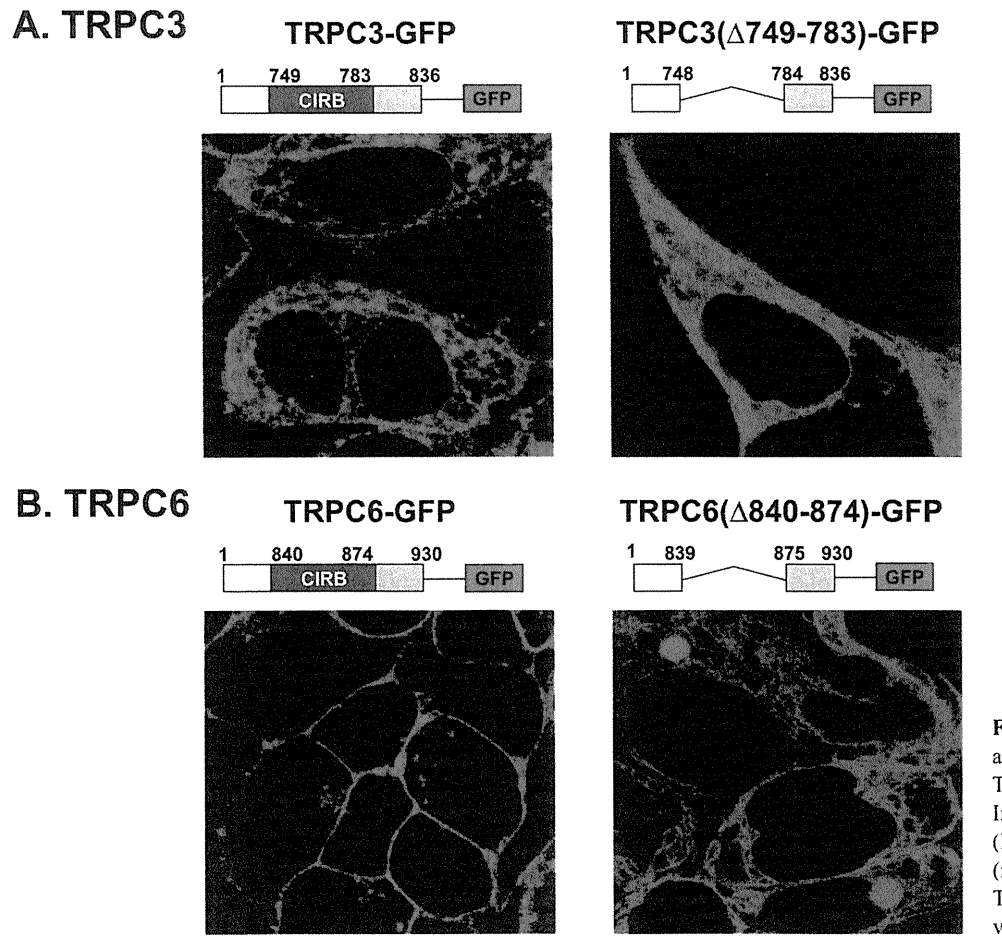

Fig. 5. Significance of CIRB domain at the C terminus of TRPC3 (A) and TRPC6 (B) in subcellular localization. Intracellular distribution of wild type (left column) and deletion mutants (right column) for TRPC3 (A) and TRPC6 (B) under basal condition was visualized by confocal microscopy.

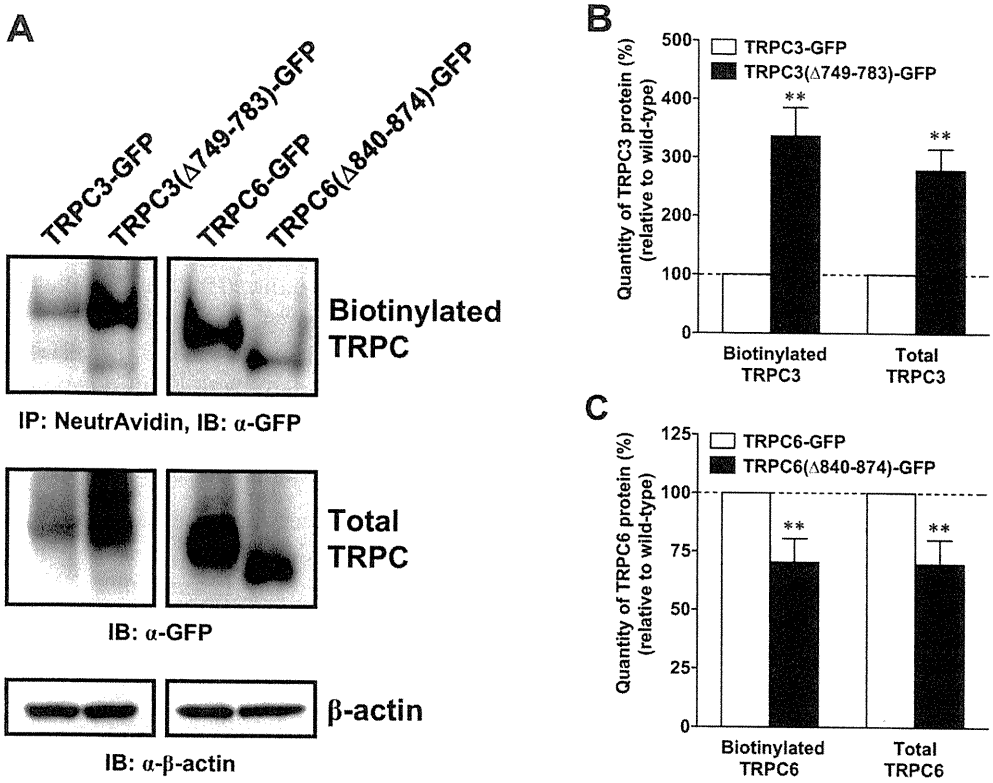

Fig. 6. Surface biotinylation of wild-type and CIRB domain deletion mutant TRPC3-GFP and TRPC6-GFP. A: The upper panel is a western blot containing the proteins that bound and eluted from agarose-linked NeutrAvidin to estimate biotinylated TRPC proteins. The middle panel is a western blot for whole cell lysates to estimate total TRPC proteins. The lower panel is a western blot for whole cell lysates to estimate the internal control (β-actin). These blots were probed with monoclonal antibodies as indicated (IB). B and C: The histogram represents the relative ratios of cell surface and of total proteins in mutant TRPC3 (B) and TRPC6 (C) to those in wild-type TRPC3 and TRPC6, respectively. The ratios were normalized by the quantity of β-actin. Data are presented as the mean ± S.E.M. of the results obtained from 4 experiments. $^{**}P < 0.01$ vs. its wild type.

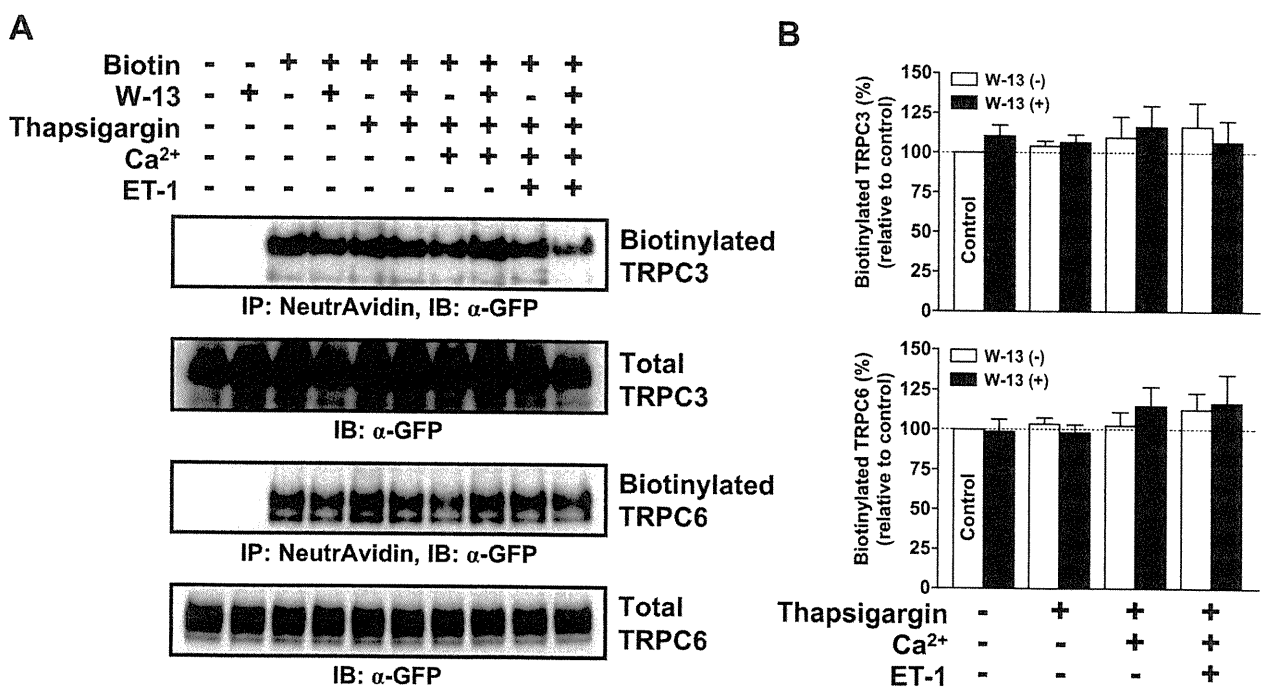

Fig. 7. Effects of W-13 on cell surface localization of wild-type TRPC3-GFP and TRPC6-GFP. A: Some of the extracts were prepared from cells treated with the drugs as indicated prior to cell surface labeling with biotin. Cells were treated with or without 10 μM W-13 for 30 min at 37°C, and then 2 μM TG, 2 μM Ca^{2+}, and 10 nM ET-1 was subsequently added to the culture media according to the protocol for the Ca^{2+} measurement study shown in Fig. 1. B: The histograms represent the relative ratios of cell surface proteins in wild-type TRPC3 (upper panel) and TRPC6 (lower panel) to those in wild-type TRPC3 and TRPC6, respectively. The ratios of cell surface TRPC protein levels were normalized by the quantity of total TRPC proteins. Data are presented as the mean ± S.E.M. of the results obtained from 4 experiments.

channels and that DAG-sensitive TRPC3, TRPC6, and TRPC7 form ROCC rather than SOCC (32, 33). However, there is conflicting evidence on whether each TRPC isoforms form SOCC or ROCE, e.g., TRPC3 is reported to form SOCC (34) while other studies indicate that TRPC3 acts as ROCC independently of SOCC activation (11, 35). Furthermore, the expression level of TRPC3 is important to determine its activation mechanisms: TRPC3 functions as a ROCC at higher levels of expression, while it is activated by the depletion of ER at relatively low levels of expression (36).

In the present study, we first explored TRPC isoforms functioning as ET_AR-activated ROCCs in HEK293 cells stably coexpressing HA-ET_AR and one of the TRPC tagged with GFP at the C terminus, since Ca^{2+} entry via TRPC is particularly an important stimulus for the development of cardiovascular diseases such as IPAH associated with excessive stimulation of ET_AR (6). To estimate ROCE, we added 10 μM Gd^{3+} to the extracellular medium to inhibit SOCE that masks the ROCE (19). However, 10 μM Gd^{3+} did not completely inhibit SOCE triggered by TG-induced Ca^{2+}-depletion/Ca^{2+}-restoration. It is well-known that TRPC proteins can form heteromultimeric channels that function as SOCCs. Since HEK293 cells express native TRPC1, TRPC3, TRPC4, TRPC6, and TRPC7 (37), there is the possibility that the TRPC3 and TRPC6 exogenously expressed in HEK293 cells also form Gd^{3+}-resistant heteromultimers in combination with the endogenous TRPC proteins, of which some can trigger Gd^{3+}-insensitive SOCE. Using this experimental condition with 10 μM Gd^{3+}, we found that TRPC3, TRPC5, TRPC6, and TRPC7 are operated upon ET_AR stimulation in the cells whose SOCE had been triggered by the TG-induced ER depletion/Ca^{2+}-restoration protocol (Fig. 1). In addition, there was no significant difference in the ET_AR-operated Ca^{2+} entry via TRPC3 and TRPC6 between wild-type and GFP-tagged TRPC, when transiently expressed in the HEK293 cells (data not shown). These results suggest that augmentation of Ca^{2+} entry via these TRPC isoforms in response to ET_AR stimulation occurs independently of the depletion of ER and that the C-terminal fusion with GFP does not affect the TRPC-mediated Ca^{2+} entry. The observation that TRPC3, TRPC5, TRPC6, and TRPC7 function as ROCCs (Fig. 1) is basically consistent with the evidence for the involvement of store-independent mechanisms in the regulation of TRPC3 (38), TRPC5 (38), TRPC6 (25), and TRPC7 (19). Among the ET_AR-operated TRPC channels identified in this study, G_q/PLC-dependent activation of TRPC3 and TRPC6 is a particularly important mechanism underlying Ca^{2+} responses to ET-1 in cardiovascular systems (2, 3, 26, 27, 39).

Remarkably, unlike the ROCE via TRPC3, the TRPC6-mediated ROCE was not associated with a sustained Ca^{2+} entry phase after the transient Ca^{2+} entry (Fig. 1). In addition, the function of TRPC6 as a ROCC was not observed (Supplementary Fig. 1B), when Ca^{2+} influx was triggered by the ET-1–induced Ca^{2+} release from the ER/Ca^{2+}-restoration protocol. This may result from the inactivation of TRPC6 by an ET_AR-activated signaling molecule(s). In contrast to TRPC6, the TRPC3-mediated, Gd^{3+}-insensitive Ca^{2+} influx induced by the ET-1–induced Ca^{2+} release/Ca^{2+}-restoration was unexpectedly strong as compared to the TRPC3-mediated ROCE (Fig. 1C), indicating the possibility that activity of TRPC3 is potentiated by ET_AR stimulation. Future studies are needed to identify the mechanisms underlying modulation of TRPC activity after stimulation of ET_AR.

Stimulation of ET_AR induces Ca^{2+} release from ER and Ca^{2+} influx via SOCC and/or ROCC, resulting in increases in $[Ca^{2+}]_i$ (21 – 23, 40). Intracellular Ca^{2+} can activate CaM that is a ubiquitous intracellular Ca^{2+}-binding protein involved in the Ca^{2+}-dependent regulation of numerous proteins including TRPC channels (41). CaM competes with IP_3R for binding to the CIRB domain at the C terminus of any TRPC in a Ca^{2+}-dependent manner (16, 17). CaM is reported to be critical for the regulation of TRPC channels and its role is different depending on channel isoforms (see "Introduction").

Unlike the previous reports (16, 18), the present findings clearly indicate that TRPC3 and TRPC6 were activated by Ca^{2+} and CaM. That is, ET_AR-mediated ROCE and OAG-induced Ca^{2+} influx via TRPC3 and TRPC6 were inhibited by W-13, a CaM antagonist. TRPC3(Δ749-783)-GFP and TRPC6(Δ840-874)-GFP, both of which lack the CIRB domain, can no longer trigger ROCE in responses to ET-1 and OAG. Notably, with the biotinylation assay, there was no change in the proportion of cell surface expression of these mutant TRPC channels to total cell expression following the deletion of the CIRB domain, although the total cell expression level of the mutant TRPC channels was slightly altered (Fig. 6C). In addition, CaM inhibition by W-13 did not alter the cell surface expression of TRPC channels (Fig. 7). These data taken together indicate that the channel function of TRPC3 and TRPC6 is positively regulated by CaM binding to the CIRB domain of these TRPC channels, and they also indicate that this positive regulation is not due to translocation of these channel molecules to the plasma membrane but probably due to alterations of channel function itself. There are two possible mechanisms for activation of TRPC3 and TRPC6 by CaM. First, CaM binding itself to the CIRB domain of either TRPC3 or TRPC6 results in allosteric regulation of channel activity, as previously suggested for TRPC6 in human platelets (14). Alternatively, TRPC3 and TRPC6 require their

phosphorylation by CaM-dependent protein kinase II for activation (42).

In addition to regulation of TRPC channel activity by CaM binding, there is a previous report that implicates a role of the CIRB domain of TRPC3 in translocation between the cell surface and intracellular compartments (13). This study based on confocal microscopic imaging suggests that deletion of the CIRB domain changes the subcellular distribution of TRPC3 from the cell surface to ER/Golgi (13). We also observed a similar change in subcellular distribution for CIRB deletion mutants of TRPC6, TRPC6(⊿840-874)-GFP (Fig. 5B), using confocal microscopic imaging. However, in sharp contrast with confocal microscopic findings, our cell surface biotinylation experiments have clearly revealed that the mutant TRPC3 and TRPC6 proteins lacking the CIRB domain show no substantial change in the proportion of cell surface expression to total cell expression, in comparison with that of wild-type TRPC channels, as described above. The reason for the discrepancy between the biotinylation study and confocal microscopic study is at present unknown, but it is probably due to the intrinsic property of confocal microscopic study that quantification of target proteins expressed on the plasma membrane is virtually impossible.

In summary, we have demonstrated that four TRPC isoforms, TRPC3, TRPC5, TRPC6, and TRPC7, can function as ET_AR-operated Ca^{2+} channels. Both TRPC3- and TRPC6-mediated ROCE in response to ET_AR stimulation are positively regulated by G_q protein, PLC, and CaM. The CIRB domain present in the C terminus of TRPC3 and TRPC6 is important for channel activation, which is performed through CaM binding to the domain but not translocation of TRPC channels to the cell surface.

Acknowledgments

We thank Dr. Yasuo Mori (Kyoto University, Kyoto) for kindly donating vectors encoding TRPC constructs. We also thank Astellas Pharma, Inc. (Tokyo) for generously providing YM-254890. This study was supported in part by a Grant-in-Aid for Young Scientists (B) from Japan Society for the Promotion of Science [grant 21790236] (to T. Horinouchi); a Grant-in-Aid for Scientific Research (B) from Japan Society for the Promotion of Science [grant 21390068] (to S.M.); and grants from Smoking Research Foundation of Japan (to S.M.), Mitsubishi Pharma Research Foundation (to T. Horinouchi), the Pharmacological Research Foundation, Tokyo (to T. Horinouchi), the Shimabara Science Promotion Foundation (to T. Horinouchi), and Actelion Pharmaceuticals Japan Ltd. (to T. Horinouchi).

References

1 Miwa S, Kawanabe Y, Okamoto Y, Masaki T. Ca^{2+} entry channels involved in endothelin-1-induced contractions of vascular smooth muscle cells. J Smooth Muscle Res. 2005;41:61–75.

2 Kuwahara K, Nakao K. New molecular mechanisms for cardiovascular disease: transcriptional pathways and novel therapeutic targets in heart failure. J Pharmacol Sci. 2011;116:337–342.

3 Nishida M. Roles of heterotrimeric GTP-binding proteins in the progression of heart failure. J Pharmacol Sci. 2011;117:1–5.

4 Berridge MJ, Bootman MD, Roderick HL. Calcium signalling: dynamics, homeostasis and remodelling. Nat Rev Mol Cell Biol. 2003;4:517–529.

5 Spassova MA, Soboloff J, He LP, Hewavitharana T, Xu W, Venkatachalam K, et al. Calcium entry mediated by SOCs and TRP channels: variations and enigma. Biochim Biophys Acta. 2004;1742:9–20.

6 Abramowitz J, Birnbaumer L. Physiology and pathophysiology of canonical transient receptor potential channels. FASEB J. 2009;23:297–328.

7 Kawanabe Y, Okamoto Y, Miwa S, Hashimoto N, Masaki T. Molecular mechanisms for the activation of voltage-independent Ca^{2+} channels by endothelin-1 in Chinese hamster ovary cells stably expressing human $endothelin_A$ receptors. Mol Pharmacol. 2002;62:75–80.

8 Iwamuro Y, Miwa S, Minowa T, Enoki T, Zhang XF, Ishikawa M, et al. Activation of two types of Ca^{2+}-permeable nonselective cation channel by endothelin-1 in A7r5 cells. Br J Pharmacol. 1998;124:1541–1549.

9 Iwamuro Y, Miwa S, Zhang XF, Minowa T, Enoki T, Okamoto Y, et al. Activation of three types of voltage-independent Ca^{2+} channel in A7r5 cells by endothelin-1 as revealed by a novel Ca^{2+} channel blocker LOE 908. Br J Pharmacol. 1999;126:1107–1114.

10 Vazquez G, Wedel BJ, Aziz O, Trebak M, Putney JWJ. The mammalian TRPC cation channels. Biochim Biophys Acta. 2004;1742:21–36.

11 Hofmann T, Obukhov AG, Schaefer M, Harteneck C, Gudermann T, Schultz G. Direct activation of human TRPC6 and TRPC3 channels by diacylglycerol. Nature. 1999;397:259–263.

12 Schaefer M, Plant TD, Obukhov AG, Hofmann T, Gudermann T, Schultz G. Receptor-mediated regulation of the nonselective cation channels TRPC4 and TRPC5. J Biol Chem. 2000;275:17517–17526.

13 Wedel BJ, Vazquez G, McKay RR, St J Bird G, Putney JWJ. A calmodulin/inositol 1,4,5-trisphosphate (IP_3) receptor-binding region targets TRPC3 to the plasma membrane in a calmodulin/IP_3 receptor-independent process. J Biol Chem. 2003;278:25758–25765.

14 Dionisio N, Albarran L, Berna-Erro A, Hernandez-Cruz JM, Salido GM, Rosado JA. Functional role of the calmodulin- and inositol 1,4,5-trisphosphate receptor-binding (CIRB) site of TRPC6 in human platelet activation. Cell Signal. 2011;23:1850–1856.

15 Singh BB, Liu X, Tang J, Zhu MX, Ambudkar IS. Calmodulin regulates Ca^{2+}-dependent feedback inhibition of store-operated Ca^{2+} influx by interaction with a site in the C terminus of TrpC1. Mol Cell. 2002;9:739–750.

16 Zhang Z, Tang J, Tikunova S, Johnson JD, Chen Z, Qin N, et al. Activation of Trp3 by inositol 1,4,5-trisphosphate receptors through displacement of inhibitory calmodulin from a common binding domain. Proc Natl Acad Sci U S A. 2001;98:3168–3173.

17 Tang J, Lin Y, Zhang Z, Tikunova S, Birnbaumer L, Zhu MX.

Identification of common binding sites for calmodulin and inositol 1,4,5-trisphosphate receptors on the carboxyl termini of trp channels. J Biol Chem. 2001;276:21303–21310.

18 Kwon Y, Hofmann T, Montell C. Integration of phosphoinositide- and calmodulin-mediated regulation of TRPC6. Mol Cell. 2007;25:491–503.

19 Okada T, Inoue R, Yamazaki K, Maeda A, Kurosaki T, Yamakuni T, et al. Molecular and functional characterization of a novel mouse transient receptor potential protein homologue TRP7. Ca^{2+}-permeable cation channel that is constitutively activated and enhanced by stimulation of G protein-coupled receptor. J Biol Chem. 1999;274:27359–27370.

20 Yee JK, Friedmann T, Burns JC. Generation of high-titer pseudotyped retroviral vectors with very broad host range. Methods Cell Biol. 1994;43:99–112.

21 Horinouchi T, Nishimoto A, Nishiya T, Lu L, Kajita E, Miwa S. Endothelin-1 decreases $[Ca^{2+}]_i$ via Na^+/Ca^{2+} exchanger in CHO cells stably expressing endothelin ET_A receptor. Eur J Pharmacol. 2007;566:28–33.

22 Higa T, Horinouchi T, Aoyagi H, Asano H, Nishiya T, Nishimoto A, et al. Endothelin type B receptor-induced sustained Ca^{2+} influx involves $G_{q/11}$/phospholipase C-independent, p38 mitogen-activated protein kinase-dependent activation of Na^+/H^+ exchanger. J Pharmacol Sci. 2010;113:276–280.

23 Horinouchi T, Asano H, Higa T, Nishimoto A, Nishiya T, Muramatsu I, et al. Differential coupling of human endothelin type A receptor to $G_{q/11}$ and G_{12} proteins: the functional significance of receptor expression level in generating multiple receptor signaling. J Pharmacol Sci. 2009;111:338–351.

24 Bradford MM. A rapid and sensitive method for the quantitation of microgram quantities of protein utilizing the principle of protein-dye binding. Anal Biochem. 1976;72:248–254.

25 Boulay G. Ca^{2+}-calmodulin regulates receptor-operated Ca^{2+} entry activity of TRPC6 in HEK-293 cells. Cell Calcium. 2002; 32:201–207.

26 Yu Y, Fantozzi I, Remillard CV, Landsberg JW, Kunichika N, Platoshyn O, et al. Enhanced expression of transient receptor potential channels in idiopathic pulmonary arterial hypertension. Proc Natl Acad Sci U S A. 2004;101:13861–13866.

27 Kunichika N, Landsberg JW, Yu Y, Kunichika H, Thistlethwaite PA, Rubin LJ, et al. Bosentan inhibits transient receptor potential channel expression in pulmonary vascular myocytes. Am J Respir Crit Care Med. 2004;170:1101–1107.

28 Lussier MP, Lepage PK, Bousquet SM, Boulay G. RNF24, a new TRPC interacting protein, causes the intracellular retention of TRPC. Cell Calcium. 2008;43:432–443.

29 Morimoto YV, Kojima S, Namba K, Minamino T. M153R mutation in a pH-sensitive green fluorescent protein stabilizes its fusion proteins. PLoS One. 2011;6:e19598.

30 Seibel NM, Eljouni J, Nalaskowski MM, Hampe W. Nuclear localization of enhanced green fluorescent protein homomultimers. Anal Biochem. 2007;368:95–99.

31 Watanabe H, Murakami M, Ohba T, Takahashi Y, Ito H. TRP channel and cardiovascular disease. Pharmacol Ther. 2008;118: 337–351.

32 Yuan P, Leonetti MD, Pico AR, Hsiung Y, MacKinnon R. Structure of the human BK channel Ca^{2+}-activation apparatus at 3.0 A resolution. Science. 2010;329:182–186.

33 Villereal ML. Mechanism and functional significance of TRPC channel multimerization. Semin Cell Dev Biol. 2006;17:618–629.

34 Kiselyov K, Xu X, Mozhayeva G, Kuo T, Pessah I, Mignery G, et al. Functional interaction between $InsP_3$ receptors and store-operated Htrp3 channels. Nature. 1998;396:478–482.

35 Ma HT, Patterson RL, van Rossum DB, Birnbaumer L, Mikoshiba K, Gill DL. Requirement of the inositol trisphosphate receptor for activation of store-operated Ca^{2+} channels. Science. 2000; 287:1647–1651.

36 Vazquez G, Wedel BJ, Trebak M, St John Bird G, Putney JWJ. Expression level of the canonical transient receptor potential 3 (TRPC3) channel determines its mechanism of activation. J Biol Chem. 2003;278:21649–21654.

37 Worley PF, Zeng W, Huang GN, Yuan JP, Kim JY, Lee MG, et al. TRPC channels as STIM1-regulated store-operated channels. Cell Calcium. 2007;42:205–211.

38 Venkatachalam K, Zheng F, Gill DL. Regulation of canonical transient receptor potential (TRPC) channel function by diacylglycerol and protein kinase C. J Biol Chem. 2003;278:29031–29040.

39 Xi Q, Adebiyi A, Zhao G, Chapman KE, Waters CM, Hassid A, et al. IP_3 constricts cerebral arteries via IP_3 receptor-mediated TRPC3 channel activation and independently of sarcoplasmic reticulum Ca^{2+} release. Circ Res. 2008;102:1118–1126.

40 Horinouchi T, Miyake Y, Nishiya T, Nishimoto A, Morishima S, Muramatsu I, et al. Functional role of Na^+/H^+ exchanger in Ca^{2+} influx mediated via human endothelin type A receptor stably expressed in Chinese hamster ovary cells. J Pharmacol Sci. 2008;107:456–459.

41 Zhu MX. Multiple roles of calmodulin and other Ca^{2+}-binding proteins in the functional regulation of TRP channels. Pflugers Arch. 2005;451:105–115.

42 Shi J, Mori E, Mori Y, Mori M, Li J, Ito Y, et al. Multiple regulation by calcium of murine homologues of transient receptor potential proteins TRPC6 and TRPC7 expressed in HEK293 cells. J Physiol. 2004;561:415–432.

1521-0103/12/3401-143–151$25.00
THE JOURNAL OF PHARMACOLOGY AND EXPERIMENTAL THERAPEUTICS

JPET 340:143–151, 2012

Vol. 340, No. 1
187500/3738844

Adenylate Cyclase/cAMP/Protein Kinase A Signaling Pathway Inhibits Endothelin Type A Receptor-Operated Ca^{2+} Entry Mediated via Transient Receptor Potential Canonical 6 Channels[S]

Takahiro Horinouchi, Tsunaki Higa, Hiroyuki Aoyagi, Tadashi Nishiya, Koji Terada, and Soichi Miwa

Department of Cellular Pharmacology, Hokkaido University Graduate School of Medicine, Hokkaido, Japan

Received August 31, 2011; accepted October 13, 2011

ABSTRACT

Receptor-operated Ca^{2+} entry (ROCE) via transient receptor potential canonical channel 6 (TRPC6) is important machinery for an increase in intracellular Ca^{2+} concentration triggered by the activation of G_q protein-coupled receptors. TRPC6 is phosphorylated by various protein kinases including protein kinase A (PKA). However, the regulation of TRPC6 activity by PKA is still controversial. The purpose of this study was to elucidate the role of adenylate cyclase/cAMP/PKA signaling pathway in the regulation of G_q protein-coupled endothelin type A receptor (ET_AR)-mediated ROCE via TRPC6. For this purpose, human embryonic kidney 293 (HEK293) cells stably coexpressing human ET_AR and TRPC6 (wild type) or its mutants possessing a single point mutation of putative phosphorylation sites for PKA were used to analyze ROCE and amino acids responsible for PKA-mediated phosphorylation of TRPC6. Ca^{2+} measurements with thapsigargin-induced Ca^{2+}-depletion/Ca^{2+}-restoration protocol to estimate ROCE showed that the stimulation of ET_AR induced marked ROCE in HEK293 cells expressing TRPC6 compared with control cells. The ROCE was inhibited by forskolin and papaverine to activate the cAMP/PKA pathway, whereas it was potentiated by Rp-8-bromoadenosine-cAMP sodium salt, a PKA inhibitor. The inhibitory effects of forskolin and papaverine were partially cancelled by replacing Ser28 ($TRPC6^{S28A}$) but not Thr69 ($TRPC6^{T69A}$) of TRPC6 with alanine. In vitro kinase assay with Phos-tag biotin to determine the phosphorylation level of TRPC6 revealed that wild-type and mutant ($TRPC6^{S28A}$ and $TRPC6^{T69A}$) TRPC6 proteins were phosphorylated by PKA, but the phosphorylation level of these mutants was lower (approximately 50%) than that of wild type. These results suggest that TRPC6 is negatively regulated by the PKA-mediated phosphorylation of Ser28 but not Thr69.

Introduction

Ca^{2+} signaling regulates various important physiological and pathophysiological events, including cell constriction, cell proliferation, cell differentiation, and activation of immune cells. Increased Ca^{2+} influx via transient receptor potential canonical channel 6 (TRPC6), a voltage-independent, Ca^{2+}-permeable nonselective cation channel, is particularly a major stimulus for the development of cardiovascular diseases, such as idiopathic pulmonary arterial hypertension (IPAH), which is associated with the continued stimulation of endothelin type A receptor (ET_AR) resulting from excessive

This study was supported in part by Grants-in-Aid for Young Scientists (B) from the Japan Society for the Promotion of Science [grant 21790236] (to T. Horinouchi); Grants-in-Aid for Scientific Research (B) from the Japan Society for the Promotion of Science [grant 21390068] (to S.M.); and grants from the Smoking Research Foundation of Japan (to S.M.), the Mitsubishi Pharma Research Foundation (to T. Horinouchi), the Pharmacological Research Foundation, Tokyo (to T. Horinouchi), the Shimabara Science Promotion Foundation (to T. Horinouchi), and Actelion Pharmaceuticals Japan Ltd. (to T. Horinouchi).

Article, publication date, and citation information can be found at http://jpet.aspetjournals.org.

http://dx.doi.org/10.1124/jpet.111.187500.

[S] The online version of this article (available at http://jpet.aspetjournals.org) contains supplemental material.

ABBREVIATIONS: TRPC, transient receptor potential canonical; AC, adenylate cyclase; BSA, bovine serum albumin; $[Ca^{2+}]_i$, intracellular free Ca^{2+} concentration; ECL, enhanced chemiluminescence; EPAC, exchange protein activated by cAMP; ER, endoplasmic reticulum; ET-1, endothelin-1; ET_AR, endothelin type A receptor; fura-2/AM, fura-2/acetoxymethyl ester; GFP, green fluorescent protein; G_qPCR, G_q protein-coupled receptor; HA, hemagglutinin; HEK293, human embryonic kidney 293; HRP, horseradish peroxidase; IB, immunoblotting; IP, immunoprecipitation; IPAH, idiopathic pulmonary arterial hypertension; PDE, phosphodiesterase; PKA, protein kinase A; PKG, protein kinase G; ROCC, receptor-operated Ca^{2+} channel; ROCE, receptor-operated Ca^{2+} entry; Rp-8-Br-cAMP, Rp-8-bromoadenosine-cAMP sodium salt; SA, streptavidine; SOCE, store-operated Ca^{2+} entry; SQ-22,536, 9-(tetrahydro-2-furanyl)-9*H*-purin-6-amine; TG, thapsigargin; WT, wild type.

production of endothelin-1 (ET-1) (Abramowitz and Birnbaumer, 2009). TRPC6 has been identified as a potential candidate for a receptor-operated Ca^{2+} channel (ROCC) rather than a store-operated Ca^{2+} channel, and it is operated by phospholipase C-mediated diacylglycerol production after stimulation of G_q protein-coupled receptors (G_qPCRs) such as α_1-adrenergic and angiotensin type I receptors (Watanabe et al., 2008). However, it remains unclear whether the activation of G_q protein-coupled ET_AR with its agonist, ET-1, triggers ROCE through TRPC6.

The activity of TRPC6 is positively and negatively regulated by various protein kinases: the channel is activated by Ca^{2+}/calmodulin-dependent protein kinase II and the Src tyrosine kinase family (Hisatsune et al., 2004; Shi et al., 2004), whereas it is inactivated by protein kinase C and protein kinase G (PKG) (Kim and Saffen, 2005; Kinoshita et al., 2010; Nishida et al., 2010). TRPC6 is also phosphorylated by protein kinase A (PKA), which is a downstream target of cAMP, whereas PKA-mediated phosphorylation of TRPC6 is reported not to affect channel function (Hassock et al., 2002). However, Nishioka et al. (2011) have shown that PKA-mediated phosphorylation of TRPC6 at Thr69 is essential for the vasorelaxant effects of phosphodiesterase type 3 (PDE3) inhibition against the angiotensin II-induced constriction of vascular smooth muscle cells. In contrast to the negative regulation of TRPC6 activity by PKA-mediated phosphorylation, cAMP is reported to activate TRPC6 via the phosphoinositide 3-kinase/protein kinase B/mitogen-activated protein kinase kinase/extracellular signal-regulated kinase 1/2 signaling pathway (Shen et al., 2011). Thus, post-translational modification of TRPC6 by protein kinases plays a critical role in the regulation of channel activity.

Drug therapy designed to elevate intracellular contents of cAMP and cGMP with G_s protein-coupled prostaglandin I_2 receptor agonists (e.g., beraprost) and cGMP-specific PDE5 inhibitors (e.g., sildenafil), respectively, is highly effective against IPAH, which is closely correlated with either the prolonged activation of ET_AR or the augmentation of Ca^{2+} influx through up-regulated TRPC6 (Kunichika et al., 2004; Yu et al., 2004). Many lines of evidence indicate that the PKA- and PKG-dependent phosphorylation of TRPC6 at Thr69 inhibits channel activity, leading to vasorelaxant and antihypertrophic effects, respectively (Kinoshita et al., 2010; Nishida et al., 2010; Nishioka et al., 2011). In terms of the substrate specificity of PKA, a study with an oriented peptide library has demonstrated that PKA is an arginine-directed serine/threonine protein kinase, and arginine residue is preferred at positions −4 to −1 amino terminal to the phosphorylation site (Songyang et al., 1994). In addition, the greatest selectivity was observed at residues −3 and −2, that is, R_2-X-S/T, and the lysine residue at the −2 position was the second preferred amino acid (R-L-X-S/T) (Songyang et al., 1994). Searching for the primary sequence of TRPC6, we have found that, in addition to the R-R-Q-T sequence surrounding Thr69, potential sequences for PKA-mediated phosphorylation are present within the TRPC6 sequence, namely R-R-G-G-S at Ser14, R-R-N-E-S at Ser28, and R-K-L-S at Ser321. Unlike Thr69, which is responsible for PKA-mediated negative regulation of TRPC6 activity (Nishioka et al., 2011), there is no conclusive evidence for the functional role of these serine residues in the regulation of TRPC6 activity by PKA.

In the present study, we tried to clarify whether TRPC6 functions as ET_AR-operated Ca^{2+} channels by using Ca^{2+} measurements with a thapsigargin (TG)-induced Ca^{2+}-depletion/Ca^{2+}-restoration protocol. In addition, we made and used TRPC6 mutants possessing a single point mutation of putative phosphorylation sites for PKA to identify key amino acids responsible for the regulation of TRPC6 activity by PKA-mediated phosphorylation. For this purpose, we improved an in vitro kinase assay by using Phos-tag biotin (a phosphate-specific ligand with biotin tag) to detect specifically phosphorylated proteins (Kinoshita et al., 2006). We here show that, although PKA can phosphorylate TRPC6 on Ser28 and Thr69, ET_AR-operated Ca^{2+} entry through TRPC6 is negatively regulated by the activation of the AC/cAMP/PKA signaling pathway, via phosphorylation of TRPC6 on Ser28 but not on Thr69 of the N terminus.

Materials and Methods

Materials. The following drugs and reagents were used in the present study: synthetic human ET-1 (Peptide Institute Inc., Osaka, Japan); fura-2/acetoxymethyl ester (fura-2/AM) and Pluronic F-127 (Dojindo Laboratories, Kumamoto, Japan); gadolinium (III) chloride, G418, TG, probenecid, aprotinin, leupeptin, pepstatin, sodium deoxycholate, SDS, phenylmethylsulfonyl fluoride, Na_3VO_4, NaF, puromycin dihydrochloride, forskolin, 1,9-dideoxyforskolin, 8-bromoadenosine-cAMP, papaverine hydrochloride, ATP, and bovine serum albumin (BSA) (Sigma-Aldrich, St. Louis, MO); Rp-8-bromoadenosine-cAMP sodium salt (Rp-8-Br-cAMP) and 8-(4-chlorophenylthio)-2′-*O*-methyladenosine-cAMP sodium salt (Enzo Life Sciences Inc., Plymouth Meeting, PA); SQ-22,536 [9-(tetrahydro-2-furanyl)-9*H*-purin-6-amine] (Calbiochem, San Diego, CA), cAMP-dependent protein kinase catalytic subunit (Promega, Madison, WI); and rapid alkaline phosphatase (Roche Applied Science, Mannheim, Germany). All cell culture media and supplements, except fetal calf serum (Invitrogen, Carlsbad, CA), were obtained from Sigma-Aldrich. Antibodies for FLAG peptide, a green fluorescent protein (GFP), glyceraldehyde-3-phosphate dehydrogenase, horseradish peroxidase (HRP)-conjugated FLAG peptide (HRP-FLAG), and HRP-conjugated streptavidine (HRP-SA) were obtained from Sigma-Aldrich, Clontech (Mountain View, CA), Santa Cruz Biotechnology Inc. (Santa Cruz, CA), Medical and Biological Laboratories Co., Ltd. (Aichi, Japan), and Thermo Fisher Scientific (Waltham, MA), respectively. Phos-tag biotin was obtained from NARD Institute, Ltd. (Hyogo, Japan). The other reagents used were of the highest grade in purity.

Construction of Retrovirus Vectors. The pCI-neo mammalian expression vector encoding TRPC6 (pCI-neo-TRPC6) was generously provided by Dr. Yasuo Mori (Kyoto University, Kyoto, Japan). The insert cDNA of wild-type TRPC6 was generated from the pCI-neo-TRPC6 as a template by a polymerase chain reaction with specific primers containing the restriction enzyme sites, which are BamHI at the 5′ end and AgeI at the 3′ end, for subcloning into the pCR-Blunt II-TOPO vector (Invitrogen). The resulting pCR-Blunt II-TOPO vector and the pEGFP-N1 vector encoding a red-shifted variant of GFP (Clontech) were digested with two restriction enzymes (BamHI/AgeI, AgeI/NotI, or BamHI/NotI) simultaneously. The cDNA fragments were ligated into the BamHI/NotI-treated pMXrmv5 retrovirus vector to yield the pMXrmv5 vectors encoding GFP and TRPC6 fused with GFP at the C terminus (TRPC6-GFP). All of the constructs were verified by DNA sequencing.

To identify the target sites of TRPC6 for phosphorylation by PKA, serine residues at positions 14, 28, and 321, and threonine at 69 were replaced with alanine by using a KOD-Plus- Mutagenesis Kit (Toyobo Co., Ltd., Osaka, Japan). The sequences of the resulting mutants tagged with GFP or FLAG peptide at the C terminus were confirmed by DNA sequencing.

Cell Culture. Human embryonic kidney 293 (HEK293) cells were cultured in Dulbecco's modified Eagle's medium supplemented with 10% (v/v) fetal calf serum, penicillin (100 units · ml^{-1}), and streptomycin (100 μg · ml^{-1}) at 37°C in humidified air with 5% CO_2.

Stable Expression of Human ET_AR in HEK293 Cells. The pDisplay mammalian expression vector containing cDNA of human ET_AR fused with an influenza hemagglutinin (HA) epitope tag at the N terminus (HA-ET_AR) was transfected into HEK293 cells by using a TransIT-293 transfection kit (Mirus Bio Corporation, Madison, WI) according to the manufacturer's instructions. Stable transformants were selected in medium containing 800 μg · ml^{-1} G418 for 3 weeks. Clonal cell lines were obtained by limiting dilution. Clones were expanded and screened for expression levels by whole-cell radioligand binding assay and Western blot analysis. The resulting suitable clone (HA-ET_AR/HEK293 cells) was grown up for further experiments.

Stable Expression of TRPC6 and Its Mutants. To generate HA-ET_AR-positive HEK293 cells stably expressing GFP, TRPC6-GFP, TRPC6-FLAG, or their mutants, these genes were introduced into HA-ET_AR/HEK293 cells by retroviral gene transfer. In brief, retroviruses were produced by triple transfection of HEK293T cells with retroviral constructs along with gag-pol and vesicular stomatitis virus G glycoprotein expression constructs (Yee et al., 1994). The supernatants containing virus were collected 24 h after transfection and added to HA-ET_AR/HEK293 cells. The HA-ET_AR/HEK293 cells were then centrifuged at 900*g* for 45 min at 25°C followed by incubation for 6 h at 37°C in 5% CO_2 and 95% air. Then, fresh culture media were added to dilute supernatants containing virus. GFP- or TRPC6-positive HA-ET_AR/HEK293 cells were selected for growth in medium containing 5 μg · ml^{-1} puromycin for 1 week.

Measurement of Intracellular Free Ca^{2+} Concentration. Intracellular free Ca^{2+} concentration ($[Ca^{2+}]_i$) was monitored by using a fluorescent Ca^{2+} indicator, fura-2/AM, as described previously (Horinouchi et al., 2009; Higa et al., 2010). In brief, HEK293 cells grown in 3.5-cm dishes were incubated with 4 μM fura-2/AM admixed with 2.5 mM probenecid and 0.04% Pluronic F-127 at 37°C for 45 min under reduced light. After collecting and washing cells, the cells were suspended in Ca^{2+}-free Krebs-HEPES solution (140 mM NaCl, 3 mM KCl, 1 mM $MgCl_2 \cdot 6H_2O$, 11 mM D-(+)-glucose, and 10 mM HEPES, adjusted to pH 7.3 with NaOH) at 4×10^5 cells · ml^{-1}. $CaCl_2$ was added to 0.5-ml aliquots of the cell suspension at a final concentration of 2 mM, when necessary. Changes of $[Ca^{2+}]_i$ in cells were measured at 30°C by using a CAF-110 spectrophotometer (Jasco, Tokyo, Japan) with the excitation wavelengths of 340 and 380 nm and emission wavelength of 500 nm.

Confocal Microscopy. Confocal microscopy was carried out by using a FluoView FV300 microscope (Olympus, Tokyo, Japan) with a 63× oil-immersion lens.

In Vitro Kinase Assay. Wild-type and mutant TRPC6-FLAG protein-expressed HA-ET_AR/HEK293 cells grown in 10-cm dishes were washed twice with ice-cold PBS and lysed in radioimmunoprecipitation assay buffer (150 mM NaCl, 1.5 mM $MgCl_2$, 50 mM Tris-HCl, pH 6.8, 1% nonidet P-40, 0.5% sodium deoxycholate, 0.1% SDS, 1 mM phenylmethylsulfonyl fluoride, 1 mM Na_3VO_4, 20 mM NaF, 10 μg · ml^{-1} leupeptin, 10 μg · ml^{-1} aprotinin, and 10 μg · ml^{-1} pepstatin) supplemented with EDTA-free, protease inhibitor cocktail (Thermo Fisher Scientific). The cell lysates were sonicated for 10 s on setting 10 of a handy sonicator (UR-20P; Tomy Seiko Co., Ltd., Tokyo, Japan) and centrifuged at 20,000*g* for 20 min at 4°C. Protein content of supernatant was measured according to the method of Bradford (1976) using BSA as standard. Immunoprecipitation was carried out with an immunoprecipitation kit (Dynabeads Protein G; Invitrogen). In brief, the Dynabeads were incubated with a primary antibody (anti-FLAG, 1:100 dilution) for 1 h at room temperature. The Dynabeads-antibody complex was washed twice with washing buffer (150 mM NaCl, 1.5 mM $MgCl_2$, 50 mM Tris-HCl, pH 6.8, 1% nonidet P-40, 0.5% sodium deoxycholate, and 0.1% SDS) by gentle pipetting, and then incubated with lysates containing equal protein amounts for 1 h at room temperature. Western blot analysis showed that the expression of TRPC6 proteins relative to total protein was quantitatively similar between wild-type and mutant proteins (Supplemental Fig. S1). The resulting Dynabeads were washed three times with the washing buffer. The Dynabeads-binding TRPC6 proteins were then incubated with alkaline phosphatase for 1 h at 37°C to reduce basal phosphorylation levels. After being rinsed with the washing buffer three times, the dephosphorylated TRPC6 proteins were incubated in phosphorylation buffer [20 mM Tris-HCl, pH 8.0, 5 mM $MgCl_2$, 0.1 mM ATP, and cAMP-dependent protein kinase catalytic subunit (40 units per reaction)] at 37°C for 30 min. This amount of cAMP-dependent protein kinase catalytic subunit produced approximately 50% response of the maximum TRPC6 phosphorylation (Supplemental Fig. S2). The TRPC6 proteins bound to the Dynabeads were eluted in the phosphorylation buffer by adding SDS sample buffer (62.5 mM Tris-HCl, pH 6.8, 10% glycerol, 5% 2-mercaptoethanol, 2.5% SDS, and 0.1% bromphenol blue) followed by incubation at 37°C for 30 min. The phosphorylation levels of TRPC6 protein were analyzed by Western blotting.

Western Blot Analysis. The proteins in immunoprecipitated samples and whole-cell lysates were separated on a 5 to 20% polyacrylamide gel (SuperSep; Wako Pure Chemicals, Osaka, Japan) and electrotransferred to a polyvinylidene fluoride membrane (Immobilon-P; pore size 0.45 μm; Millipore Corporation, Billerica, MA) with a semidry electroblotter. After transfer, the membranes were washed three times for 5 min with Tris-buffered saline-Tween 20 (10 mM Tris-HCl, pH 8.0, 100 mM NaCl, and 0.1% Tween 20) followed by blocking (2% BSA in Tris-buffered saline-Tween 20) of nonspecific binding for 1 h at room temperature. The membranes were incubated with anti-FLAG-HRP antibody or Phos-tag biotin-bound HRP-SA complex (which was prepared according to the instructions of the manufacturer, Nard Institute, Ltd.) at room temperature for 6 h or with a monoclonal antibody for GFP or glyceraldehyde-3-phosphate dehydrogenase as a primary antibody overnight at 4°C. The anti-FLAG-HRP antibody and Phos-tag biotin-bound HRP-SA complex were detected with an ECL Western blotting Analysis System (GE Healthcare, Little Chalfont, Buckinghamshire, UK). The primary antibody was detected with a secondary horseradish peroxidase-conjugated anti-mouse IgG antibody and enhanced chemiluminescence (GE Healthcare). The blots were exposed to Amersham Hyperfilm ECL (GE Healthcare). Phosphorylation levels of wild-type and mutant TRPC6 proteins were analyzed with Image J1.37 software (National Institutes of Health, Bethesda, MD).

Data Analysis. Data regarding change in $[Ca^{2+}]_i$ were collected and analyzed by using a MacLab/8s with Chart (v. 3.5) software (ADInstruments Japan, Tokyo, Japan). All data are presented as means ± S.E.M. where *n* refers to the number of experiments. The significance of the difference between mean values was evaluated with Prism (version 3.00; GraphPad Software Inc., San Diego, CA) by Student's paired or unpaired *t* test. A P value < 0.05 was considered to indicate significant differences.

Results

Characterization of ET_AR-Operated Ca^{2+} Entry through TRPC6. To determine whether the stimulation of ET_AR with its agonist, ET-1, induces ROCE via TRPC6, we used the TG-induced Ca^{2+}-depletion/Ca^{2+}-restoration protocol to measure store-operated Ca^{2+} entry (SOCE) followed by ET_AR stimulation to measure ROCE (Boulay, 2002). Gd^{3+} (10 μM) in the extracellular medium was used throughout the experiments to inhibit the endogenous SOCE (capacitative Ca^{2+} entry) that masks the ROCE via TRPC3 and TRPC7 in HEK293 cells (Okada et al., 1999). In GFP- and TRPC6-GFP-expressing HA-ET_AR/HEK293 cells, SOCE induced by TG-induced Ca^{2+} depletion/Ca^{2+} restoration was significantly inhibited by the addition of 10 μM Gd^{3+}

(210.2 ± 11.5 to 46.0 ± 2.1 nM for GFP and 177.2 ± 4.8 to 41.2 ± 1.9 nM for TRPC6-GFP; n = 6 for each). Figure 1 shows that in nominally Ca^{2+}-free solution containing 10 μM Gd^{3+} 2 μM TG evoked Ca^{2+} release from the endoplasmic reticulum (ER), causing a transient increase in $[Ca^{2+}]_i$ that promptly returned to near baseline. In the TG-treated HA-ET_AR/HEK293 cells expressing GFP as a control, stimulation with 10 nM ET-1 after restoration of extracellular Ca^{2+} to 2 mM did not produce a further increase in $[Ca^{2+}]_i$ (Fig. 1A), indicating that under this condition ET_AR stimulation cannot elicit either Ca^{2+} release from Ca^{2+} store, SOCE, or ROCE. On the other hand, the stimulation of ET_AR with 10 nM ET-1 elicited a Gd^{3+}-insensitive transient increase in $[Ca^{2+}]_i$ resulting from ROCE through TRPC6 in the TG-treated HA-ET_AR/HEK293 cells expressing TRPC6-GFP (Fig. 1B; Table 1). These results clearly suggest that the activation of ET_AR is able to elicit ROCE mediated through TRPC6-GFP.

Negative Regulation of ET_AR-Operated, TRPC6-Mediated Ca^{2+} Entry by the Activation of Adenylate Cyclase/cAMP/Protein Kinase A Signaling Pathway. Next, we examined the effects of cAMP and PKA on TRPC6-mediated ROCE in response to ET_AR stimulation. The ROCE was markedly suppressed by either 10 μM forskolin, an AC activator (Fig. 2B), or 10 μM papaverine, a nonselective PDE inhibitor (Fig. 2D), both of which increase the intracellular cAMP level, thereby activating PKA. The inhibitory effect of forskolin on TRPC6-mediated ROCE was cancelled by treatment with 1 mM SQ-22,536, a membrane-permeable AC inhibitor, that also weakly but significantly augmented the ROCE (Supplemental Fig. S3). Because it is well known that forskolin can exhibit pleiotropic effects in an AC-independent manner (Laurenza et al., 1989), we examined the effect of 1,9-dideoxyforskolin, an inactive analog of forskolin as a negative control (Pinto et al., 2008, 2009), on the ET_AR-operated Ca^{2+} influx via TRPC6. We were surprised to find that 10 μM 1,9-dideoxyforskolin as well as 10 μM forskolin inhibited the TRPC6-mediated Ca^{2+} entry (Supplemental Fig. S3). The inhibitory effect of 10 μM 1,9-dideoxyforskolin was cancelled by 1 mM SQ-22,536, indicating the possibility that 1,9-dideoxyforskolin was able to directly activate AC. Rp-8-Br-cAMP (100 μM), a membrane-permeable PKA inhibitor, enhanced

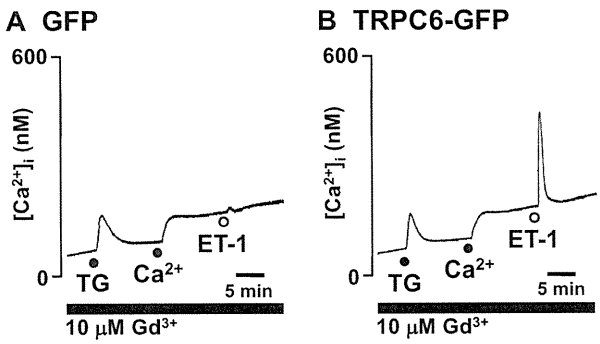

Fig. 1. Characterization of ROCE induced by the activation of ET_AR in HEK293 cells stably coexpressing human ET_AR and TRPC6-GFP. Representative traces for TG-induced SOCE and ET_AR-activated ROCE after store depletion in the presence of 10 μM Gd^{3+} in GFP-transfected (A) and TRPC6-GFP-transfected (B) HEK293 cells stably expressing human ET_AR are shown. TG (2 μM)-induced Ca^{2+} release from ER in nominally Ca^{2+}-free medium was followed by SOCE upon restoration of 2 mM extracellular Ca^{2+}. ROCE was triggered by the stimulation of ET_AR with 10 nM ET-1 12 min after the addition of extracellular Ca^{2+}.

TABLE 1

Comparison of ET_AR-operated Ca^{2+} entry mediated through wild-type and mutant TRPC6 in HEK293 cells stably coexpressing human ET_AR and TRPC6 proteins

Results are presented as means ± S.E.M. of n number of experiments. Sequences represent amino acids at amino-terminal to phosphorylation sites for PKA. $[Ca^{2+}]_{iMAX}$ (nM) is the peak of ROCE induced by 10 nM ET-1.

Mutation	Sequences	n	$[Ca^{2+}]_{iMAX}$
			nM
Wild type		8	266.4 ± 40.1
S14A	R-R-G-G-S^{14}	6	243.8 ± 32.6
S28A	R-R-N-E-S^{28}	7	247.4 ± 26.6
T69A	R-R-Q-T^{69}	7	282.8 ± 27.6
S321A	R-K-L-S^{321}	6	221.0 ± 38.8

S, serine; A, alanine; T, threonine; G, glycine; N, asparagine; E, Glutamic acid; Q, glutamine; K, lysine; L, leucine.

ET_AR-operated Ca^{2+} influx (Fig. 2C), whereas 500 μM 8-bromoadenosine-cAMP, a membrane-permeable direct PKA activator, suppressed the Ca^{2+} response to ET-1 (Supplemental Fig. S3). The effects of these drugs on ET_AR-induced ROCE via TRPC6 are summarized in Fig. 2E and Supplemental Fig. S3. Our findings indicate the possibility that the activity of TRPC6 is negatively regulated by its phosphorylation by PKA, resulting in the inhibition of ET_AR-operated Ca^{2+} entry via TRPC6.

Effect of Activation of cAMP/PKA Signaling Pathway on Subcellular Localization of TRPC6. Wild-type TRPC6 protein expressed in HEK293 cells is reported to be mainly present on the plasma membrane (Lussier et al., 2008; Graham et al., 2010). We confirmed the subcellular localization of TRPC6-GFP expressed in HA-ET_AR/HEK293 cells under basal conditions by using a confocal laser-scanning microscopic approach. Although GFP expressed in HA-ET_AR/HEK293 cells as a control was localized in the cytosol and nucleus (Fig. 3A), wild-type TRPC6-GFP was predominantly targeted to the plasma membrane (Fig. 3B). The intracellular distribution of GFP and TRPC6-GFP after treatment with 10 μM forskolin (Fig. 3, C and D), and 10 μM papaverine (Fig. 3, E and F) was similar to that in the control cells. Likewise, pharmacological inhibition of AC and PKA with 1 mM SQ-22,536 and 100 μM Rp-8-Br-cAMP, respectively, did not seem to affect the intracellular distribution of GFP and TRPC6-GFP (Supplemental Fig. S4).

Determination of the Amino Acid Residue Responsible for the Inhibition of TRPC6-Mediated Ca^{2+} Influx by Forskolin and Papaverine. To determine the critical amino acid residues involved in the inhibition of ROCE via TRPC6 by forskolin and papaverine, we searched for the PKA phosphorylation candidate sites in the TRPC6 sequence. As a result, we found three serine residues at positions 14 (R-R-G-G-S), 28 (R-R-N-E-S), and 321 (R-K-L-S) and a single threonine residue at 69 (R-R-Q-T): all of these sequences were present on the intracellular N-terminal region of TRPC6. To identify the target residues of PKA phosphorylation, we made HA-ET_AR/HEK293 cells stably expressing GFP-tagged TRPC6 mutants carrying an alanine substitution for these serine/threonine residues. Functional study with Ca^{2+} measurement demonstrated that there was no significant difference in the magnitude of ROCE between wild type and these mutants (Table 1). Replacement of Ser28 (S28A) but not other residues (Ser14, Thr69, and Ser321) by alanine (S14A, T69A, and S321A) attenuated the inhibitory effects of 10 μM forskolin

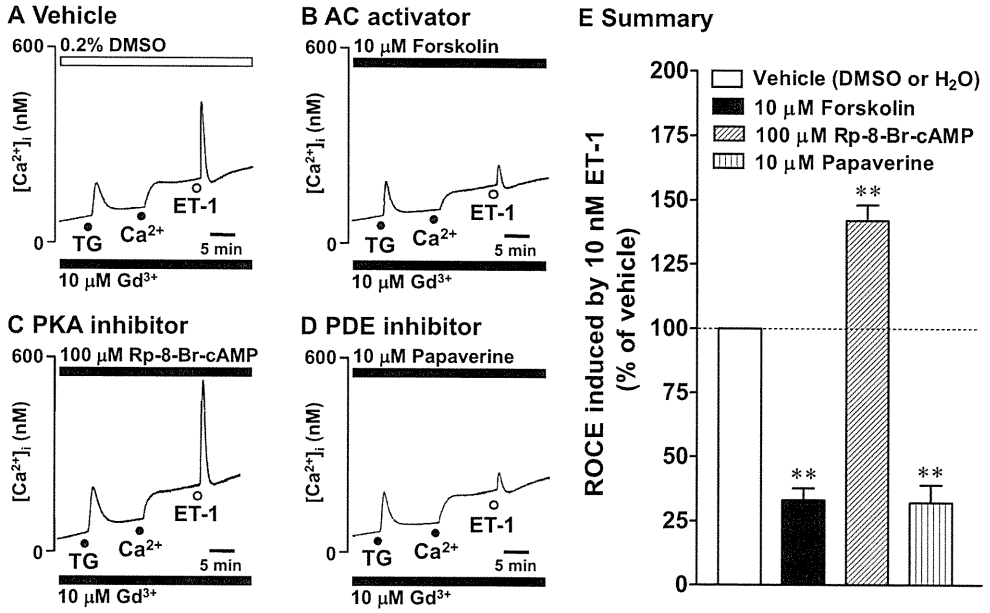

Fig. 2. A to D, effects of DMSO (A), forskolin (B), Rp-8-Br-cAMP (C), and papaverine (D) on ROCE via TRPC6-GFP induced by 10 nM ET-1. Data are presented as means ± S.E.M of the results obtained from four to six experiments. E, summary of results. **, $P < 0.01$, versus vehicle.

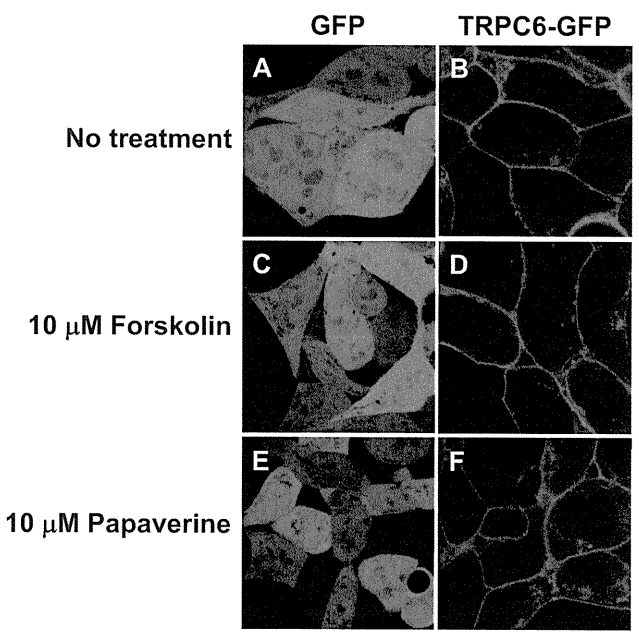

Fig. 3. C to F, effects of forskolin and papaverine on the intracellular distribution of GFP (C and E) and TRPC6-GFP (D and F) expressed in ET_AR/HEK293 cells. The cells were treated with 10 μM forskolin (C and D) and 10 μM papaverine (E and F) for 30 min. A and B, no treatment for GFP (A) and TRPC6-GFP (B). The subcellular localization of GFP and TRPC6-GFP was visualized by fluorescence confocal microscopy.

(Fig. 4, A and B) and 10 μM papaverine (Fig. 5, A and B). The effects of these drugs on ET_AR-induced ROCE via wild-type and mutant TRPC6 proteins are summarized in Figs. 4C and 5C.

Identification of PKA Phosphorylation Sites on TRPC6 by Using In Vitro Kinase Assay with Phos-Tag Biotin. To directly demonstrate that TRPC6 is a substrate for PKA, PKA-mediated phosphorylation of TRPC6 was estimated by using Phos-tag biotin, which is a biotinylated phosphate-specific ligand that can specifically detect phosphorylated proteins (Kinoshita et al., 2006). Figure 6A shows that immunoblotting with Phos-tag biotin-bound HRP-SA complex detected wild-type and mutant phosphorylated TRPC6 proteins under basal conditions, which were reduced by treatment of immunoprecipitated TRPC6 proteins with phosphatase, indicating the ability of Phos-tag biotin to specifically identify phosphorylated proteins. The basal phosphorylation level of wild-type TRPC6 was similar to that of mutant TRPC6 proteins (Fig. 6A). To analyze a change in the levels of TRPC6 phosphorylation by PKA in vivo, the HA-ET_AR/HEK293 cells stably expressing wild-type or mutant TRPC6-FLAG protein were treated with a combination of 10 μM forskolin and 10 μM papaverine to enhance cAMP production and inhibit cAMP breakdown by PDE, respectively. However, there was little or no change in the phosphorylation levels of wild-type and mutant TRPC6 after the activation of the AC/cAMP/PKA signaling pathway (Fig. 6B). We considered the possibility that the high basal phosphorylation levels masked the effects of cAMP-elevating agents. Therefore, we next attempted to perform an in vitro kinase assay on immunoprecipitated TRPC6 proteins, which were pretreated with a phosphatase to reduce their basal phosphorylation levels. Incubation with an exogenous PKA catalytic subunit induced phosphorylation of wild-type TRPC6 protein dephosphorylated with a phosphatase pretreatment (Fig. 6C, top), demonstrating that the target sites for PKA-mediated phosphorylation are present within the TRPC6 sequence. There was no significant difference in an increase in the phosphorylation level of TRPC6 protein by PKA between wild type and $TRPC6^{S14A}$ mutant. It is noteworthy that an in vitro kinase assay using TRPC6 mutants with Ser28 ($TRPC6^{S28A}$) and Thr69 ($TRPC6^{T69A}$) replaced to alanine showed significant loss of phosphorylation, suggesting that PKA can phosphorylate TRPC6 on these sites and the Ser28 and Thr69 residues contributed to approximately 50% of the phosphorylation of TRPC6 by PKA.

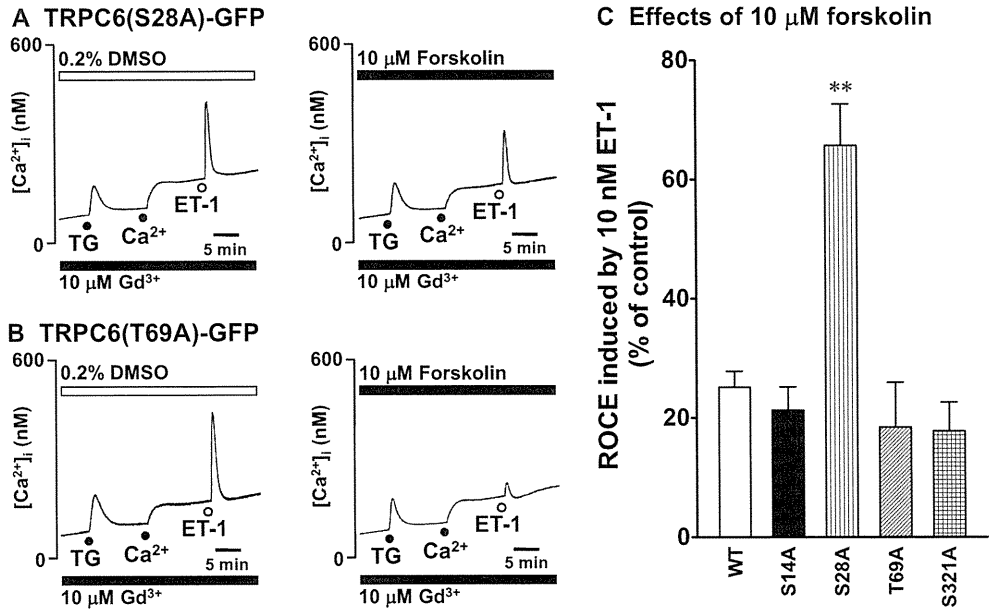

Fig. 4. Effects of alanine substitutions for putative PKA phosphorylation sites on the inhibition of ROCE via TRPC6-GFP by forskolin. A and B, representative traces for inhibitory effects of 10 μM forskolin on ROCE via TRPC6 induced by 10 nM ET-1 in TRPC6(S28A)-GFP (A) and TRPC6(T69A)-GFP (B). C, inhibitory effects of 10 μM forskolin on ROCE in response to 10 nM ET-1 in wild-type (WT) and mutants of TRPC6. Data are presented as means ± S.E.M of the results obtained from four to six experiments. **, $P < 0.01$, versus wild type.

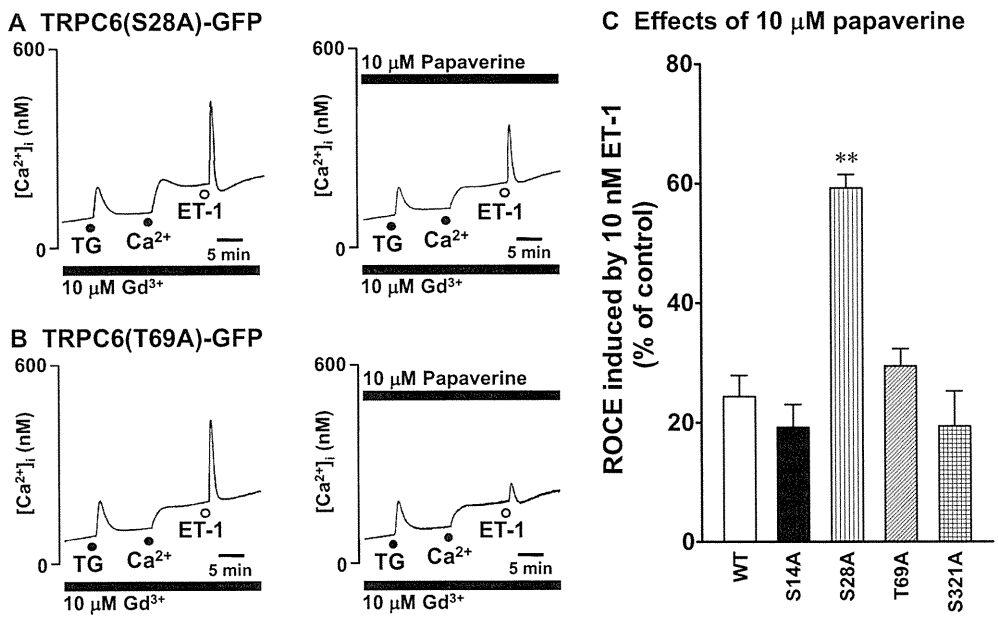

Fig. 5. Effects of alanine substitutions for putative PKA phosphorylation sites on the inhibition of ROCE via TRPC6-GFP by papaverine. A and B, representative traces for inhibitory effects of 10 μM papaverine on ROCE via TRPC6 induced by 10 nM ET-1 in TRPC6(S28A)-GFP (A) and TRPC6(T69A)-GFP (B). C, inhibitory effects of 10 μM papaverine on ROCE in response to 10 nM ET-1 in wild-type and mutants of TRPC6. Data are presented as means ± S.E.M of the results obtained from four to six experiments. **, $P < 0.01$, versus wild type.

Discussion

Activation of G_qPCR and tyrosine kinase receptor induces formation of the second messengers such as inositol 1,4,5-trisphosphate and diacylglycerol via phospholipase C. Binding of inositol 1,4,5-trisphosphate to its receptor on ER triggers Ca^{2+} release from ER, resulting in store-operated (capacitative) Ca^{2+} entry mediated through voltage-independent Ca^{2+}-permeable cation channels including TRPC and Orai proteins (Lee et al., 2010). In addition, ROCE is activated, and it is mediated via certain TRPCs categorized as ROCCs that operate independently of store depletion. TRPC6 is reported to be involved in ROCE triggered by the stimulation of G_qPCRs such as muscarinic (Bousquet et al., 2010) and α_1-adrenergic receptors (Suzuki et al., 2007). In the present study, we showed that activation of G_q protein-coupled ET_AR induced TRPC6-mediated ROCE but not SOCE. That is, an increase in $[Ca^{2+}]_i$ induced by TG-induced Ca^{2+}-depletion/Ca^{2+}-restoration in GFP-expressing cells was not significantly different from that in TRPC6-GFP-expressing cells, indicating that TRPC6 does not contribute to SOCE. Different from no significant Ca^{2+} influx in response to ET-1

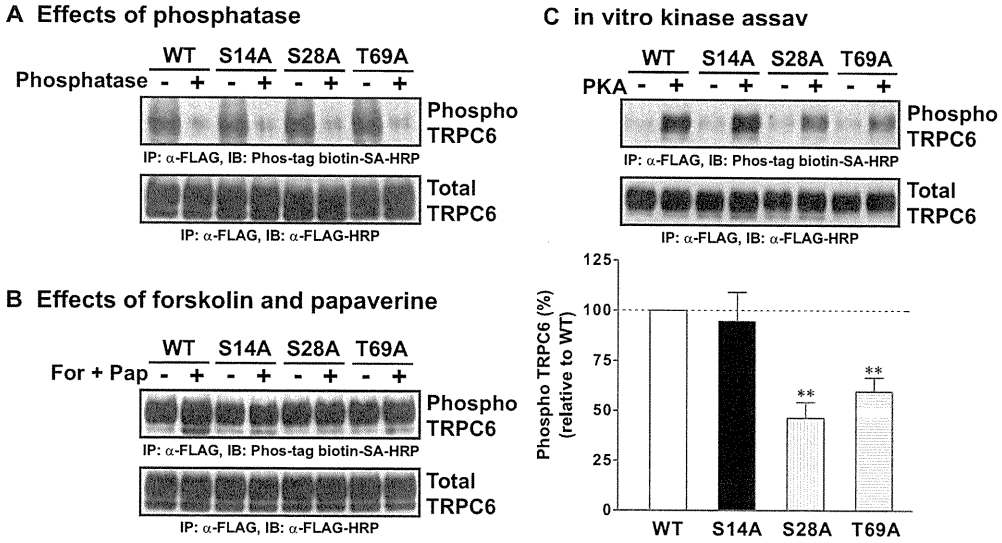

Fig. 6. Phosphorylation of wild-type and mutant TRPC6 proteins stably expressed in HA-ET_AR/HEK293 cells. Top blots are representative immunoblots with Phos-tag biotin-bound HRP-SA complex detecting phosphorylated TRPC6 proteins (indicated as phospho TRPC6). Bottom blots are representative immunoblots with anti-FLAG-HRP antibody to determine the quantity of TRPC6 in the immunoprecipitate (indicated as total TRPC6). A, effects of phosphatase treatment on the basal phosphorylation of FLAG-tagged TRPC6 proteins immunoprecipitated with anti-FLAG antibody. Immunoprecipitated TRPC6 proteins were incubated in the dephosphorylation buffer for 1 h. B, effects of forskolin and papaverine (For + Pap) on the basal phosphorylation of TRPC6-FLAG proteins in vivo. HA-ET_AR/HEK293 cells expressing wild-type and mutant TRPC6-FLAG were treated with a combination of 10 μM forskolin and 10 μM papaverine for 30 min. Subsequently, immunoprecipitation and immunoblotting of TRPC6 were performed to estimate changes in the phosphorylation level of TRPC6 proteins. C, phosphorylation of TRPC6 on Ser28 and Thr69 by PKA. Immunoprecipitated TRPC6 proteins were incubated in the PKA phosphorylation buffer for 30 min. The histogram represents the relative ratio of PKA-induced phosphorylation of mutant TRPC6 proteins to that of wild-type TRPC6. The PKA-induced phosphorylation of each sample was calculated as the ratio of the phosphorylation level of TRPC6 (phospho TRPC6) in the presence of PKA catalytic subunit to that in the absence of PKA catalytic subunit. These phosphorylation levels were normalized by the quantity of total TRPC6 protein (total TRPC6). Data are presented as means ± S.E.M of the results obtained from four experiments. **, $P < 0.01$, versus its wild type.

after TG-induced Ca^{2+}-depletion/Ca^{2+}-restoration in the GFP-expressing cells, 10 nM ET-1 was capable of producing additional Ca^{2+} influx in the TRPC6-expressing cells where SOCE had been maximally activated by TG-induced Ca^{2+} depletion/Ca^{2+} restoration. In addition, our fluorescent confocal microscopic observations were consistent with the previous report of Graham et al. (2010) showing that, unlike diffuse distribution of GFP, TRPC6-GFP is predominantly present in the plasma membrane or subplasma membrane of the cells. These data, taken together, indicate that TRPC6 located in plasma membrane functions as an ET_AR-activated ROCC but not a store-operated Ca^{2+} channel.

Other studies have indicated that the negative regulation of TRPC6 by PKA in addition to PKG is an important mechanism underlying the protective effect of cAMP-elevating agent against cardiovascular diseases such as hypertension and cardiac hypertrophy (Kinoshita et al., 2010; Nishida et al., 2010; Nishioka et al., 2011). PKA is the major target of the intracellular second-messenger cAMP, which is synthesized from ATP via AC and inactivated by some members of the PDE superfamily (Boswell-Smith et al., 2006; Pearce et al., 2010). To elucidate the functional role of AC/cAMP/PKA signaling pathway in the regulation of ET_AR-operated Ca^{2+} influx via TRPC6, we used pharmacological agents targeting this pathway. The TRPC6-mediated ROCE in response to ET_AR stimulation was markedly reduced in the presence of cAMP-elevating agents, forskolin and papaverine. In contrast, the response was significantly potentiated by pretreatment with a membrane-permeant PKA inhibitor, Rp-8-Br-cAMP, that competitively binds to the cAMP-binding domain of the PKA regulatory subunit and inhibits dissociation of the catalytic subunit from the regulatory subunit (Schwede et al., 2000). Furthermore, either forskolin or papaverine did not change the membrane localization of TRPC6 protein (Fig. 3). cAMP can activate not only PKA but also exchange protein activated by cAMP (EPAC) that functions as guanine nucleotide exchange factors for both Rap1 and Rap2, members of the Ras family of small G proteins (Gloerich and Bos, 2010). However, the possibility that cAMP-dependent EPAC activation by forskolin or papaverine inactivates TRPC6 could be ruled out, because the selective EPAC agonist, 8-(4-chlorophenylthio)-2′-*O*-methyladenosine-cAMP sodium salt (200 μM), had no or little effect on the ROCE via TRPC6 (data not shown). Taken together, these findings suggest the inactivation of ET_AR-activated TRPC6 by the AC/cAMP/PKA signaling pathway. This supports the observation by Nishioka et al. (2011) that cAMP-dependent PKA activation induced by cilostazol, a selective PDE3 inhibitor, results in the suppression of TRPC6-mediated Ca^{2+} entry. However, conflicting results have been reported on the role of cAMP-dependent signaling pathways in the regulation of TRPC6 activity. As opposed to the findings described in the present and previous studies (Nishioka et al., 2011), cAMP/PKA pathway did not affect SOCE-independent, nonselective cation entry (ROCE) via TRPC6 (Hassock et al., 2002), whereas TRPC6-mediated Ca^{2+} entry was triggered by cAMP-dependent activation of phosphoinositide 3-kinase/protein kinase B/mitogen-activated protein kinase kinase/extracellular signal-regulated kinase 1/2 signaling pathway (Shen et al., 2011). The reason for the discrepancy in these experimental results is not clear. However, the discrepancy may be attributed to the difference in the basal phosphorylation state of TRPC6, because TRPC6 is phosphorylated by several types of protein kinases under basal conditions (Fig. 6) (Bousquet et al., 2011).

It is noteworthy that we have found that 1,9-dideoxyforskolin, an inactive analog of forskolin (Pinto et al., 2008, 2009), also inhibited ET_AR-operated Ca^{2+} influx via TRPC6 (Supplemental Fig. S3). The inhibition of the ROCE by 10 μM 1,9-dideoxyforskolin seems to be caused by the activation of AC, because the inhibitory effect is sensitive to 1 mM SQ-22,536, an AC inhibitor. Other studies with purified catalytic AC subunits clearly have suggested that 1,9-dideoxyforskolin binds to AC, whereas the stimulatory activity in AC is not observed (Pinto et al., 2008, 2009). Activation of AC requires both the binding of diterpenes, including forskolin and 1,9-dideoxyforskolin, to the catalytic subunits of AC and an additional conformational switch via a yet unidentified step (Pinto et al., 2009). In native systems such as intact cells the binding of 1,9-dideoxyforskolin to AC may trigger a second conformational switch that results in the activation of catalysis.

Does the activation of PKA via AC/cAMP signaling pathway induce phosphorylation of TRPC6? Hassock et al. (2002) have reported that pharmacological stimulation of cAMP/PKA signaling pathway actually phosphorylates an unidentified phosphorylation site of TRPC6 endogenously expressed in human platelets and exogenously overexpressed in QBI-293A cells (a subclone of HEK293 cells). Other studies have shown that a Thr69 residue within the TRPC6 sequence is phosphorylated by PKA in addition to PKG (Nishida et al., 2010; Nishioka et al., 2011). We analyzed the primary sequence of TRPC6 and found some serine/threonine residues other than Thr69, i.e., Ser14, Ser28, and Ser321, as potential sites for PKA phosphorylation. Both our site-directed mutagenesis and $[Ca^{2+}]_i$ measurement experiments have provided the first functional evidence that Ser28 but not Thr69 is involved in the inhibition of TRPC6-mediated ROCE in response to ET_AR stimulation by cAMP-elevating agents.

Finally, we have conducted immunoblotting analysis with Phos-tag biotin to clarify whether PKA can phosphorylate TRPC6 on Ser28 residue. Phos-tag biotin is a phosphate-specific ligand with a biotin tag and allows us to detect specifically phosphorylated proteins (Kinoshita et al., 2006). As shown in Fig. 6A, we have confirmed that Phos-tag biotin can discriminate between phosphorylated and unphosphorylated states of TRPC6 proteins. Bousquet et al. (2011) have reported that TRPC6 protein stably expressed in HEK293 cells is phosphorylated under basal conditions and the Ser814 residue contributes to 50% of the basal phosphorylation state, although its functional significance is unknown. Our site-directed mutagenesis approach has revealed that the contribution of Ser14, Ser28, and Thr69 residues to the basal phosphorylation of TRPC6 is minor (Fig. 6, A and B). In vivo treatment of wild-type and mutant cells with a combination of forskolin and papaverine to activate PKA via the AC/cAMP signaling pathway induced little or no significant change in the phosphorylation level, indicating that the high basal phosphorylation masks the relatively weak PKA-mediated phosphorylation of TRPC6. Therefore, we have carried out an in vitro kinase assay with immunoprecipitated wild-type and mutant TRPC6 proteins that are dephosphorylated by phosphatase treatment. We were surprised to find that an in vitro kinase assay revealed that PKA phosphorylates TRPC6 on not only Ser28 but also Thr69, although only Ser28 is involved in the negative regulation of ET_AR-mediated ROCE via TRPC6 by the activation of the AC/cAMP/PKA signaling pathway. This discrepancy between $[Ca^{2+}]_i$ measurement and in vitro kinase assays could result from the fact that the Thr69 mutant of TRPC6 is functionally resistant to increased PKA activity, because Thr69 but not Ser28 is maximally phosphorylated under basal conditions. Another possibility is that the PKA catalytic subunit at 40 units used in the present study nonspecifically phosphorylates Thr69 as a PKG phosphorylation site in addition to Ser28 as a PKA phosphorylation site, because PKA and PKG are known to have very similar consensus sites.

In summary, we have identified a new phosphorylation site (Ser28) on TRPC6 for PKA in addition to Thr69. We have provided the first evidence that the activation of the AC/cAMP/PKA signaling pathway inhibits ET_AR-mediated ROCE via TRPC6 by phosphorylation of Ser28 but not Thr69, although both sites could be phosphorylated by PKA in vitro. In the treatment of IPAH attributable to excessive ET_AR signaling and/or Ca^{2+} entry via TRPC6 (Kunichika et al., 2004; Yu et al., 2004), prostacyclin and its analogs have been used as cAMP-generating drugs to relax contracted pulmonary artery and inhibit the proliferation of pulmonary artery smooth muscle cells (Clapp et al., 2002). Taken together, our findings imply that the negative regulation of ET_AR-activated TRPC6 via PKA phosphorylation may be an important therapeutic target for the treatment of PAH with cAMP-elevating agents.

Acknowledgments

We thank Dr. Yasuo Mori (Kyoto University, Kyoto, Japan) for kindly donating the vector encoding TRPC6 construct.

Authorship Contributions

Participated in research design: Horinouchi, Nishiya, and Miwa.
Conducted experiments: Horinouchi, Higa, Aoyagi, and Tarada.
Contributed new reagents or analytic tools: Horinouchi.
Performed data analysis: Horinouchi, Higa, and Aoyagi.
Wrote or contributed to the writing of the manuscript: Horinouchi, Nishiya, and Miwa.

References

Abramowitz J and Birnbaumer L (2009) Physiology and pathophysiology of canonical transient receptor potential channels. *FASEB J* **23:**297–328.
Boswell-Smith V, Spina D, and Page CP (2006) Phosphodiesterase inhibitors. *Br J Pharmacol* **147:**S252–S257.
Boulay G (2002) Ca^{2+}-calmodulin regulates receptor-operated Ca^{2+} entry activity of TRPC6 in HEK-293 cells. *Cell Calcium* **32:**201–207.
Bousquet SM, Monet M, and Boulay G (2010) Protein kinase C-dependent phosphorylation of transient receptor potential canonical 6 (TRPC6) on serine 448 causes channel inhibition. *J Biol Chem* **285:**40534–40543.
Bousquet SM, Monet M, and Boulay G (2011) The serine 814 of TRPC6 is phosphorylated under unstimulated conditions. *PLoS One* **6:**e18121.
Bradford MM (1976) A rapid and sensitive method for the quantitation of microgram quantities of protein utilizing the principle of protein-dye binding. *Anal Biochem* **72:**248–254.
Clapp LH, Finney P, Turcato S, Tran S, Rubin LJ, and Tinker A (2002) Differential effects of stable prostacyclin analogs on smooth muscle proliferation and cyclic AMP generation in human pulmonary artery. *Am J Respir Cell Mol Biol* **26:**194–201.
Gloerich M and Bos JL (2010) Epac: defining a new mechanism for cAMP action. *Annu Rev Pharmacol Toxicol* **50:**355–375.
Graham S, Ding M, Ding Y, Sours-Brothers S, Luchowski R, Gryczynski Z, Yorio T, Ma H, and Ma R (2010) Canonical transient receptor potential 6 (TRPC6), a redox-regulated cation channel. *J Biol Chem* **285:**23466–23476.
Hassock SR, Zhu MX, Trost C, Flockerzi V, and Authi KS (2002) Expression and role of TRPC proteins in human platelets: evidence that TRPC6 forms the store-independent calcium entry channel. *Blood* **100:**2801–2811.
Higa T, Horinouchi T, Aoyagi H, Asano H, Nishiya T, Nishimoto A, Muramatsu I, and Miwa S (2010) Endothelin type B receptor-induced sustained Ca^{2+} influx involves $G_{q/11}$/phospholipase C-independent, p38 mitogen-activated protein kinase-dependent activation of Na^+/H^+ exchanger. *J Pharmacol Sci* **113:**276–280.
Hisatsune C, Kuroda Y, Nakamura K, Inoue T, Nakamura T, Michikawa T, Mizutani A, and Mikoshiba K (2004) Regulation of TRPC6 channel activity by tyrosine phosphorylation. *J Biol Chem* **279:**18887–18894.

Horinouchi T, Asano H, Higa T, Nishimoto A, Nishiya T, Muramatsu I, and Miwa S (2009) Differential coupling of human endothelin type A receptor to $G_{q/11}$ and G_{12} proteins: the functional significance of receptor expression level in generating multiple receptor signaling. *J Pharmacol Sci* **111:**338–351.

Kim JY and Saffen D (2005) Activation of M1 muscarinic acetylcholine receptors stimulates the formation of a multiprotein complex centered on TRPC6 channels. *J Biol Chem* **280:**32035–32047.

Kinoshita E, Kinoshita-Kikuta E, Takiyama K, and Koike T (2006) Phosphate-binding tag, a new tool to visualize phosphorylated proteins. *Mol Cell Proteomics* **5:**749–757.

Kinoshita H, Kuwahara K, Nishida M, Jian Z, Rong X, Kiyonaka S, Kuwabara Y, Kurose H, Inoue R, Mori Y, et al. (2010) Inhibition of TRPC6 channel activity contributes to the antihypertrophic effects of natriuretic peptides-guanylyl cyclase-A signaling in the heart. *Circ Res* **106:**1849–1860.

Kunichika N, Landsberg JW, Yu Y, Kunichika H, Thistlethwaite PA, Rubin LJ, and Yuan JX (2004) Bosentan inhibits transient receptor potential channel expression in pulmonary vascular myocytes. *Am J Respir Crit Care Med* **170:**1101–1107.

Laurenza A, Sutkowski EM, and Seamon KB (1989) Forskolin: a specific stimulator of adenylyl cyclase or a diterpene with multiple sites of action? *Trends Pharmacol Sci* **10:**442–447.

Lee KP, Yuan JP, Hong JH, So I, Worley PF, and Muallem S (2010) An endoplasmic reticulum/plasma membrane junction: STIM1/Orai1/TRPCs. *FEBS Lett* **584:**2022–2027.

Lussier MP, Lepage PK, Bousquet SM, and Boulay G (2008) RNF24, a new TRPC interacting protein, causes the intracellular retention of TRPC. *Cell Calcium* **43:**432–443.

Nishida M, Watanabe K, Sato Y, Nakaya M, Kitajima N, Ide T, Inoue R, and Kurose H (2010) Phosphorylation of TRPC6 channels at Thr69 is required for anti-hypertrophic effects of phosphodiesterase 5 inhibition. *J Biol Chem* **285:**13244–13253.

Nishioka K, Nishida M, Ariyoshi M, Jian Z, Saiki S, Hirano M, Nakaya M, Sato Y, Kita S, Iwamoto T, et al. (2011) Cilostazol suppresses angiotensin II-induced vasoconstriction via protein kinase A-mediated phosphorylation of the transient receptor potential canonical 6 channel. *Arterioscler Thromb Vasc Biol* **31:**2278–2286.

Okada T, Inoue R, Yamazaki K, Maeda A, Kurosaki T, Yamakuni T, Tanaka I, Shimizu S, Ikenaka K, Imoto K, et al. (1999) Molecular and functional characterization of a novel mouse transient receptor potential protein homologue TRP7. Ca^{2+}-permeable cation channel that is constitutively activated and enhanced by stimulation of G protein-coupled receptor. *J Biol Chem* **274:**27359–27370.

Pearce LR, Komander D, and Alessi DR (2010) The nuts and bolts of AGC protein kinases. *Nat Rev Mol Cell Biol* **11:**9–22.

Pinto C, Hübner M, Gille A, Richter M, Mou TC, Sprang SR, and Seifert R (2009) Differential interactions of the catalytic subunits of adenylyl cyclase with forskolin analogs. *Biochem Pharmacol* **78:**62–69.

Pinto C, Papa D, Hübner M, Mou TC, Lushington GH, and Seifert R (2008) Activation and inhibition of adenylyl cyclase isoforms by forskolin analogs. *J Pharmacol Exp Ther* **325:**27–36.

Schwede F, Maronde E, Genieser H, and Jastorff B (2000) Cyclic nucleotide analogs as biochemical tools and prospective drugs. *Pharmacol Ther* **87:**199–226.

Shen B, Kwan HY, Ma X, Wong CO, Du J, Huang Y, and Yao X (2011) cAMP activates TRPC6 channels via the phosphatidylinositol 3-kinase (PI3K)-protein kinase B (PKB)-mitogen-activated protein kinase kinase (MEK)-ERK1/2 signaling pathway. *J Biol Chem* **286:**19439–19445.

Shi J, Mori E, Mori Y, Mori M, Li J, Ito Y, and Inoue R (2004) Multiple regulation by calcium of murine homologues of transient receptor potential proteins TRPC6 and TRPC7 expressed in HEK293 cells. *J Physiol* **561:**415–432.

Songyang Z, Blechner S, Hoagland N, Hoekstra MF, Piwnica-Worms H, and Cantley LC (1994) Use of an oriented peptide library to determine the optimal substrates of protein kinases. *Curr Biol* **4:**973–982.

Suzuki F, Morishima S, Tanaka T, and Muramatsu I (2007) Snapin, a new regulator of receptor signaling, augments α_{1A}-adrenoceptor-operated calcium influx through TRPC6. *J Biol Chem* **282:**29563–29573.

Watanabe H, Murakami M, Ohba T, Takahashi Y, and Ito H (2008) TRP channel and cardiovascular disease. *Pharmacol Ther* **118:**337–351.

Yee JK, Friedmann T, and Burns JC (1994) Generation of high-titer pseudotyped retroviral vectors with very broad host range. *Methods Cell Biol* **43:**99–112.

Yu Y, Fantozzi I, Remillard CV, Landsberg JW, Kunichika N, Platoshyn O, Tigno DD, Thistlethwaite PA, Rubin LJ, and Yuan JX (2004) Enhanced expression of transient receptor potential channels in idiopathic pulmonary arterial hypertension. *Proc Natl Acad Sci U S A* **101:**13861–13866.

Address correspondence to: Dr. Soichi Miwa, Department of Cellular Pharmacology, Hokkaido University Graduate School of Medicine, North 15, West 7, Sapporo-City, Hokkaido 060-8638, Japan. E-mail: smiwa@med.hokudai.ac.jp

J Pharmacol Sci 118, 275 – 287 (2012)

Journal of Pharmacological Sciences

Full Paper

Nicotine- and Tar-Free Cigarette Smoke Induces Cell Damage Through Reactive Oxygen Species Newly Generated by PKC-Dependent Activation of NADPH Oxidase

Hiroshi Asano[1], Takahiro Horinouchi[1], Yosuke Mai[1], Osamu Sawada[1], Shunsuke Fujii[1], Tadashi Nishiya[1], Masabumi Minami[2], Takahiro Katayama[2], Toshihiko Iwanaga[3], Koji Terada[1], and Soichi Miwa[1,*]

[1]*Department of Cellular Pharmacology,* [3]*Laboratory of Histology and Cytology, Graduate School of Medicine, Hokkaido University, Sapporo 060-8638, Japan*
[2]*Department of Pharmacology, Graduate School of Pharmaceutical Sciences, Hokkaido University, Sapporo 060-0812, Japan*

Received September 13, 2011; Accepted December 22, 2011

Abstract. We examined cytotoxic effects of nicotine/tar-free cigarette smoke extract (CSE) on C6 glioma cells. The CSE induced plasma membrane damage (determined by lactate dehydrogenase leakage and propidium iodide uptake) and cell apoptosis {determined by MTS [3-(4,5-dimethylthiazol-2-yl)-5-(3-carboxymethoxyphenyl)-2-(4-sulfophenyl)-2*H*-tetrazolium] reduction activity and DNA fragmentation}. The cytotoxic activity decayed with a half-life of approximately 2 h at 37°C, and it was abolished by *N*-acetyl-L-cysteine and reduced glutathione. The membrane damage was prevented by catalase and edaravone (a scavenger of $^{\bullet}OH$) but not by superoxide dismutase, indicating involvement of $^{\bullet}OH$. In contrast, the CSE-induced cell apoptosis was resistant to edaravone and induced by authentic H_2O_2 or O_2^- generated by the xanthine/xanthine oxidase system, indicating involvement of H_2O_2 or O_2^- in cell apoptosis. Diphenyleneiodonium [NADPH oxidase (NOX) inhibitor] and bisindolylmaleimide I [BIS I, protein kinase C (PKC) inhibitor] abolished membrane damage, whereas they partially inhibited apoptosis. These results demonstrate that 1) a stable component(s) in the CSE activates PKC, which stimulates NOX to generate reactive oxygen species (ROS), causing membrane damage and apoptosis; 2) different ROS are responsible for membrane damage and apoptosis; and 3) part of the apoptosis is caused by oxidants independently of PKC and NOX.
[Supplementary methods and Figure: available only at http://dx.doi.org/10.1254/jphs.11166FP]

Keywords: cigarette smoke extract (CSE), reactive oxygen species (ROS), NADPH oxidase (NOX), apoptosis, protein kinase C (PKC)

Introduction

Cigarette smoking is a major risk factor for atherosclerotic vascular diseases including stroke and coronary artery disease (1, 2), for chronic pulmonary obstructive disease (3 – 6) and for several different forms of cancer (7 – 9).

Cigarette smoke is reported to contain over 4,000 chemical constituents (10, 11). Among these are reactive oxygen species (ROS) such as peroxynitrate and free radicals of organic compounds (2, 12). Although these ROS are highly reactive, they have lifetimes of fractions of a second and are rapidly quenched during the passage of the smoke through the cigarette: thus neither of these radicals is considered to reach lungs of smokers (12).

In addition to ROS, cigarette smoke contains relatively stable substances that have the potential to stimulate production of ROS (13, 14). In this context, it has recently been reported that following exposure to cigarette smoke, cultured pulmonary artery endothelial cells generate superoxide anion (O_2^-), and it is suspected that a stable thiol-reactive compound, acrolein, is one of the candidate

*Corresponding author. smiwa@med.hokudai.ac.jp
Published online in J-STAGE on February 3, 2012 (in advance)
doi: 10.1254/jphs.11166FP

factors to trigger the generation of O_2^- (15, 16). Such stable substances could be carried throughout the systemic circulation and act in organs remote to the lungs to stimulate ROS generation (17).

Cigarette smoke can be divided into two phases, the tar (or particle)-phase and the gas-phase. The separation into two phases is usually performed by the use of a filter, typically a Cambridge glass-fiber filter that retains 99.9% of the particles larger than 0.1 micron (12). The fraction that is trapped on the filter is the tar-phase, while the fraction that goes through the filter is the gas-phase. Most of the previous works on toxic effects of cigarette smoke have been performed using either crude cigarette smoke extract (crude CSE) (15, 16, 18 – 21) or the tar phase alone (22).

The crude CSE is usually prepared by bubbling cigarette smoke in physiological salt solution and hence contains both the tar phase and gas phase. However, because the tar phase could theoretically be removed by passing the cigarette smoke through a filter like the Cambridge glass-fiber filter as described above, it is important to characterize the cytotoxic effects of the gas phase of the cigarette smoke in order to know the actual toxic effects of cigarette smoking against human health. In fact, recent works have shown that cigarette smoke extract (CSE) free of the tar phase and nicotine (nicotine- and tar-free CSE), which is prepared by bubbling cigarette smoke in salt solution after passage of it through a Cambridge glass-fiber filter, can oxidize low density lipoprotein cholesterol in vitro and promote atherosclerotic changes in aortas in vivo (23 – 25).

Our final goal is to identify the stable toxic compounds in the nicotine- and tar-free CSE that exert cytotoxic effects, to clarify the molecular mechanisms for their cytotoxic effects and to develop harmless cigarettes by removing such toxic compounds. As the first step toward this goal, we investigated the cytotoxic effects of the nicotine- and tar-free CSE and its action mechanism in cultured cells in terms of several aspects of cell damage. That is, analytical methods used in the present study were the lactate dehydrogenase (LDH) leakage assay and propidium iodide (PI) uptake for plasma membrane damage, MTS [3-(4,5-dimethylthiazol-2-yl)-5-(3-carboxymethoxyphenyl)-2-(4-sulfophenyl)-2*H*-tetrazolium] reduction assay for cell viability, and DNA fragmentation assay by agarose gel electrophoresis and TUNEL (Terminal deoxynucleotidyl transferase-mediated dUTP nick-end labeling) staining.

Materials and Methods

Materials

The cigarettes used in this study were the Hi-Lite™ brand (Japan Tobacco, Inc., Tokyo) containing 17 mg of tar and 1.4 mg of nicotine per cigarette. Mouse monoclonal antibody against rat neuronal nuclear antigen A60 (NeuN) and goat anti-mouse IgG Alexa fluor 488–conjugated secondary antibody were purchased from Invitrogen Corporation (Carlsbad, CA, USA). CytoTox-ONE™ Homogeneous Membrane Integrity Assay Kit for measurement of LDH activity, CellTiter 96™ Aqueous One Solution Cell Proliferation Assay Kit (MTS reduction assay), and Dead-End™ Fluorometric TUNEL System were from Promega Corporation (Madison, WI, USA). The reagents were purchased from the following sources: catalase, superoxide dismutase (SOD), xanthine oxidase, *N*-acetyl-L-cysteine (NAC), reduced-type glutathione (GSH), diphenyleneiodonium chloride (DPI), PI from Sigma-Aldrich Co. (St. Louis, MO, USA); edaravone (3-methyl-1-phenyl-2-pyrazolin-5-one) from Tokyo Chemical Industry Co., Ltd. (Tokyo); bisindolylmaleimide I (BIS I; 2-[1-(3-dimethylaminopropyl)-1*H*-indol-3-yl]-3-(1*H*-indol-3-yl)-maleimide), U-73122 {1-[6-((17*β*-3-methoxyestra-1,3,5(10)-trien-17-yl)amino)hexyl]-1*H*-pyrrole-2,5-dione} from Calbiochem (San Diego, CA, USA); 4′,6-diamidino-2-phenylindole dihydrochloride (DAPI), N^G-nitro-L-arginine methyl ester hydrochloride (L-NAME) from Dojindo Laboratories (Kumamoto). The other reagents were of the analytical grade in purity.

Preparation of nicotine- and tar-free CSE

The nicotine- and tar-free CSE was prepared according to the method of Yamaguchi et al. (23) with some modifications. Briefly, each cigarette was fixed horizontally to be burned, and the mainstream of the smoke was aspirated at a flow rate of 1.050 l·min^{-1}, which was strictly regulated by the KOFLOC™ mass flow controller (MODEL 8300 series; Kojima Instruments Inc., Kyoto) and passed through a Cambridge glass fiber filter (Heinr. Borgwaldt GmbH, Hamburg, Germany) to remove the tar phase of cigarette smoke and nicotine. The remaining gas phase of the smoke was bubbled into phosphate-buffered saline (PBS) at 25°C. For one experiment, the gas-phase of 40 cigarettes was bubbled into 10 ml of PBS and stored at −80°C before use. This CSE solution was defined as the concentration of 100%. A slight difference of activities between CSE samples prepared on different days was adjusted after determination of cytotoxic activity on C6 glioma cells with assays of LDH leakage and MTS reduction activity.

Co-culture of primary neurons and glia isolated from fetal rat brain

Neurons and glial cells for a co-culture system were obtained from the cerebral cortex of fetal Wistar rats

(17 – 19 days of gestation) according to the procedures described previously (26, 27). Briefly, whole cerebral cortex was isolated from a fetal rat brain and was minced using scalpel blades, and filtered through stainless steel mesh (150 mesh). The resulting single cells were seeded on glass coverslips placed on a 12-well plate (1.4×10^6 cells per ml per well) and were cultured in Eagle's Minimum Essential Medium (MEM) supplemented with L-glutamine (2 mM), D-(+)-glucose (11 mM), $NaHCO_3$ (24 mM), HEPES (10 mM), and 10% (v/v) heat-inactivated fetal calf serum (FCS, 1 – 7 days after plating) or 10% heat-inactivated horse serum (8 – 18 days after plating) at 37°C in humidified air with 5% CO_2. In order to inhibit the growth of nonneuronal cells, 10 μM cytosine arabinoside (AraC) was added for 24 h on the 6th day after seeding. This study was performed according to the Guidelines for Animal Experiments of Hokkaido University. The mature co-cultures (18 days after plating) without CSE treatment consisted of 51.3% ± 4.4% neurons and 48.7% ± 4.4% glial cells (% of average ± S.E.M.) by immunochemical staining with anti-NeuN antibody.

Evaluation of the effects of CSE on glia and neurons in co-culture system by PI staining

We evaluated the cytotoxic activity of CSE on a co-culture system by PI staining as an index of membrane damage because PI is specifically taken up into cells with membrane damage, and intercalates double-stranded nucleic acid, leading to staining of the cell nucleus (28). The neuronal and glial cells in a mature co-culture system were incubated with various concentrations of CSE for 4 h in culture medium containing PI (5 $\mu g \cdot ml^{-1}$).

After CSE treatment, neurons were identified by antibody against neuronal nuclear antigen A60 (NeuN). Briefly, the cells were washed with PBS and then fixed for 30 min at 4°C with 4% paraformaldehyde in PBS. After washing with PBS at room temperature, permeabilization was performed with 0.3% Triton X-100 in PBS (Triton/PBS) for 30 min at room temperature. After washing with Triton/PBS and blocking with 1.5% normal goat serum (Vector Laboratories, Inc., Burlingame, CA, USA), the cells were incubated with mouse anti-rat NeuN antibody (1:300) at 4°C for overnight; and on the next day, the cells were washed with Triton/PBS, followed by incubation with goat anti-mouse IgG Alexa fluor 488–conjugated secondary antibody (1:500) for 1 h at room temperature in the dark. After washing with PBS, the cells were embedded on slide glasses with VectaShield (Vector Laboratories, Inc.) containing DAPI (1:300) for staining of cellular nuclei.

The fluorescence of PI, Alexa fluor 488-NeuN, and DAPI were observed by a fluorescence microscopy (IX-71; Olympus Corporation, Tokyo) with excitation wavelengths of 530, 495, and 372 nm and emission wavelengths of 615, 519, and 456 nm, respectively. All cells were identified by nuclear staining with DAPI: among DAPI-positive cells, those cells positive for NeuN were regarded as neuronal cells, while the cells negative for NeuN, as glial cells. The cells positive for PI were regarded as cells with membrane damage. The cells were counted in three fields in each experiment, and the results were expressed as a percentage of all neurons or of all glial cells, respectively.

Culture of immortalized C6 glioma cells and evaluation of cytotoxic activity of CSE

C6 glioma cells derived from rat brain were grown as a monolayer culture in Dulbecco's modified Eagle's medium (DMEM) supplemented with 10% (v/v) heat-inactivated FCS, penicillin (100 units$\cdot ml^{-1}$) and streptomycin (100 $\mu g \cdot ml^{-1}$) at 37°C in humidified air with 5% CO_2.

We evaluated the cytotoxic activity of nicotine- and tar-free CSE on C6 glioma cells by LDH leakage, MTS reduction activity and DNA fragmentation with agarose gel electrophoresis or by TUNEL staining. C6 glioma cells were plated at a density of approximately 1×10^4 cells per well of a 96-well plate for LDH and MTS assays, 1×10^6 cells per 6-cm dish for DNA fragmentation by gel electrophoresis, or 5×10^5 cells per 3.5-cm dish for TUNEL staining. After the cells were cultured for 24 h, CSE was added to culture media at the indicated concentrations. The cells were incubated with CSE for a further 4 h in LDH and MTS assays or for 24 h in DNA fragmentation assays, unless otherwise stated. After the CSE treatment, the cells were subjected to the corresponding assays for cytotoxicity.

LDH leakage assay was performed using the CytoTox-ONE™ Homogeneous Membrane Integrity Assay Kit (Promega) according to the manufacturer's instructions. For measurement of LDH activity leaked into medium, culture medium (100 μl per well) was transferred to a new 96-well plate for the subsequent enzyme assay (Black Cliniplate; Thermo Fisher Scientific Inc., Rockford, IL, USA). For measurement of total LDH activity, the cells cultured in parallel were disrupted by adding 2 μl of Lysis Buffer to the culture medium, and subsequently, the whole lysate was transferred to the 96-well plate. The reaction was started by adding 100 μl of CytoTox-ONE™ reagent containing diaphorase and resazurin, incubated for 10 min at room temperature, and terminated by adding 50 μl of Stop Solution. The amount of the reaction product, rezorufin, was measured using a microplate reader (Fluoroskan II; Labosystems Japan, Tokyo) with an excitation wavelength of 544 nm and an

emission wavelength of 590 nm. LDH activity leaked into culture medium was represented as a percentage of the total LDH activity: LDH activity in culture media without cells was regarded as zero.

MTS reduction activity was assessed using the CellTiter 96™ Aqueous One Solution Cell Proliferation Assay Kit (Promega) according to the manufacturer's instructions. Briefly, after incubation with CSE for the indicated time, 20 μl of the kit reagent solution was added to the cell culture in a 96-well plate (100 μl of culture medium) and incubated for a further 1 h. The amount of the reduced form of MTS was measured by absorbance at 490 nm using a microplate reader (SPECTRA MAX 250; Molecular Devices Corp., Sunnyvale, CA, USA). MTS reduction activity of CSE-treated cells was represented as a percentage of the values obtained in non-treated cells (control): MTS reduction activity in culture media without cells was regarded as zero.

For analysis of DNA fragmentation by gel electrophoresis, the cells, which had been detached from the culture dish during treatment with CSE or vehicle and had been suspended in culture medium, were first collected by centrifugation of the culture medium at 400 × *g* for 10 min at 4°C. The collected cells and the cells that remained attached to the culture dish were washed with PBS, lysed by incubation with the lysis buffer [10 mM Tris-HCl (pH 7.4), 5 mM EDTA, and 0.5% Triton X-100] for 30 min at 4°C, and centrifuged at 27,000 × *g* for 15 min at 4°C. The resulting supernatants were transferred to a new set of tubes, incubated with 40 $\mu g \cdot ml^{-1}$ proteinase K for 30 min at 37°C, and extracted with phenol/chloroform (1:1 v/v). The DNA was precipitated with the conventional ethanol precipitation method. The precipitated DNA was treated with 40 $\mu g \cdot ml^{-1}$ RNase A for 30 min at 37°C. The purified DNA was subjected to gel electrophoresis on a 1.8% agarose gel at 50 mV on ice and stained with 0.5 $\mu g \cdot ml^{-1}$ ethidium bromide.

For analysis of DNA fragmentation by TUNEL staining, the cells were stained using the Dead-End™ Fluorometric TUNEL System (Promega) according to the manufacturer's instructions. Briefly, after treatment with CSE, the cells were washed with PBS and fixed with 4% paraformaldehyde in PBS for 30 min at 4°C. After washing with PBS at room temperature, the cells were permeabilized with 0.3% Triton X-100 in PBS for 30 min at room temperature. After preincubation for 10 min in Equlibration Buffer, the DNA-labeling reaction was started by adding the solution containing rTdT and fluorescein-labeled 12-dUTP, incubated for 60 min at 37°C, and terminated by adding Stop Solution. After washing with PBS, the fluorescence of fluorescein-labeled 12-dUTP was observed by fluorescence microscopy with an excitation wavelength at 490 nm and emission wavelength at 520 nm.

Data analysis

All data are presented as means ± S.E.M. The significance of the difference between mean values was evaluated with GraphPad PRISM™ (version 3.00; GraphPad Software Inc., San Diego, CA, USA) by Student's paired, unpaired *t*-test, or one-way ANOVA, followed by the Tukey multiple comparison test. A *P*-value less than 0.05 was considered to indicate statistically significant differences.

Results

Comparison of sensitivity of various cells to nicotine- and tar-free CSE

We first compared the sensitivity of various cultured cells to nicotine- and tar-free CSE (Fig. 1). All types of the cells except RAW264.7 cells were sensitive to the CSE, with C6 glioma cells being the most sensitive. In C6 glioma cells, LDH leakage was observed at the CSE concentration of 2% and reached the maximal level at 2.5%, with the EC_{50} value being around 2.2% (Fig. 1A). In CHO cells and HEK293 cells, the the EC_{50} values for LDH leakage were larger, that is, around 3.6% and 4.4%, respectively. In contrast, in RAW264.7 cells, no LDH leakage was observed. Essentially similar results were obtained for MTS reduction activity, except that in RAW264.7 cells, MTS reduction activity was increased

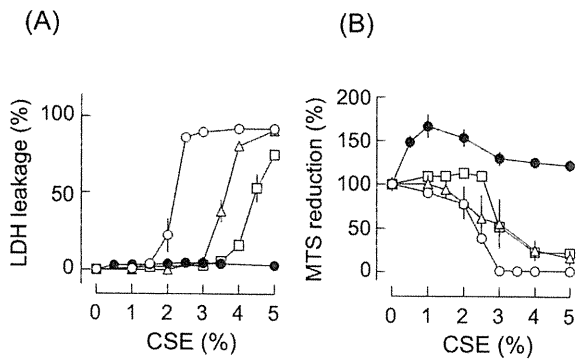

Fig. 1. Effects of varying concentrations of CSE on LDH leakage (A) and MTS reduction activity (B) in various cells. After the cells were cultured for 24 h, nicotine- and tar-free cigarette smoke extract (CSE) was added to culture medium at the indicated concentrations and incubated for a further 4 h. After the treatment, the cells were subjected to LDH leakage (A) and MTS reduction assays (B). LDH activity leaked into culture medium was represented as a percentage of the total LDH activity. MTS reduction activity of the CSE-treated cells was represented as a percentage of the values obtained in vehicle-treated cells. Data are presented as means ± S.E.M. of the values from three experiments, each in triplicate. Open circles, C6 glioma cells; open triangles, CHO cells; open squares, HEK293 cells; closed circles, RAW264.7 cells.

at low concentrations of CSE (Fig. 1B).

Glial cells are more sensitive to CSE than neurons

Because C6 glioma cells showed the highest sensitivity to CSE, we prepared a primary co-culture of glial cells and neurons from fetal rat brain and compared their sensitivity to CSE (Fig. 2). The cytotoxic effects of CSE were assessed by staining with PI, which was specifically taken up into cells with membrane damage and intercalated between double stranded DNA, leading to staining of the cell nucleus. As shown in Fig. 2A, the number of PI-stained cells was markedly increased following treatment with CSE for 4 h at concentrations of either 1.5% or 2.0% but not 1.0%. Glial cells that were identified by negative staining for NeuN were more sensitive than neurons that were positive for NeuN. That is, the proportion of the damaged cells among all glial cells was higher than that of the damaged cells among all neurons (Fig. 2B). Because glial cells were more sensitive to CSE than neurons, we decided to use an immortalized rat glioma cell line, C6 glioma cells, as a cell model in the following experiments.

Time course for LDH leakage and half-life of CSE

We examined the time course of the cytotoxic effects of CSE in C6 glioma cells (Fig. 3A). In C6 glioma cells incubated with vehicle alone, LDH leakage was unchanged up to 24 h. In contrast, when the cells were incubated with 5% CSE, LDH leakage was significantly increased at 60-min and reached a plateau of approximately 90% at 2 h.

To get insights into the chemical properties of cytotoxic factors in CSE, we attempted to estimate the half-life of the cytotoxic activity in CSE (Fig. 3B). For this purpose, CSE was preincubated at 4°C, 25°C, or 37°C for various times (2 – 24 h) without the cells: after the preincubation, it was added to the cell culture and 4 h later, LDH leakage from the cells was measured (Fig. 3B). When CSE was preincubated at 37°C, the cytotoxic activity in CSE was lost within the 4-h preincubation with a half-life of approximately 2 h. When the preincubation temperature was lower, the rate of a decrease in cytotoxic activity in CSE was slower: at 25°C, complete loss of the activity was observed at 24-h preincubation, and at 4°C, 70% of the activity remained even at 24-h preincubation. Considering that the half-life of ROS is very short (of the order of milliseconds) (12), these results indicate that the cytotoxic activity of CSE is not be

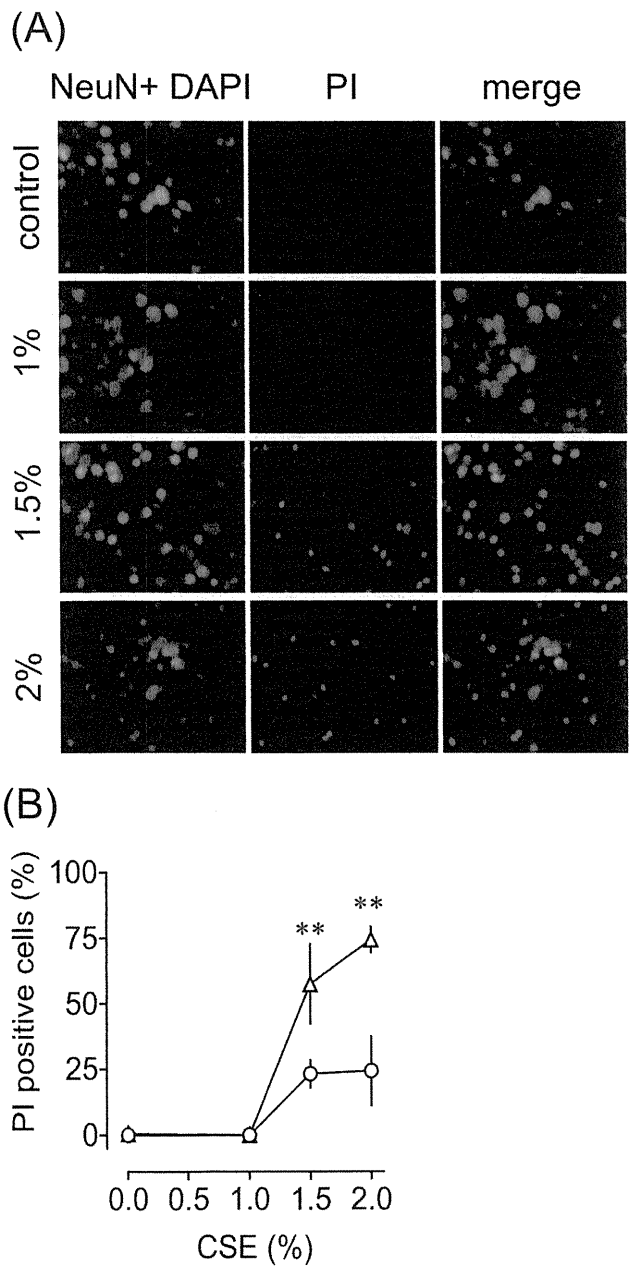

Fig. 2. Effects of varying concentrations of CSE on neurons and glial cells in co-culture prepared from fetal rat brains. A) Co-culture of neurons and glial cells were prepared from fetal rat brains as described in Materials and Methods, and it was incubated with the indicated concentrations of CSE for 4 h in the presence of propidium iodide (PI) for identification of the cells with membrane damage. After the incubation, the cells were fixed, permeabilized, and incubated with anti-rat NeuN antibody followed by anti-mouse IgG Alexa 488–labeled secondary antibody for identification of neurons. Cell nuclei were stained with DAPI upon embedding. Among DAPI-positive cells, the cells positive for NeuN were regarded as neuronal cells, while those negative for NeuN were regarded as glial cells. The fluorescence of DAPI (blue), Alexa488-NeuN (green), and PI (red) were observed by a fluorescence microscopy with excitation/emission wavelengths of 530/615, 495/519, and 372/456 nm, respectively. B) The cells were counted in three fields in each experiment, and the percentages of PI-positive neurons (open circles) and glial cells (open triangles) were expressed as a percentage of all neurons and all glial cells, respectively. Data are presented as means ± S.E.M. of the values from three experiments. $^{**}P < 0.01$ vs. neurons.

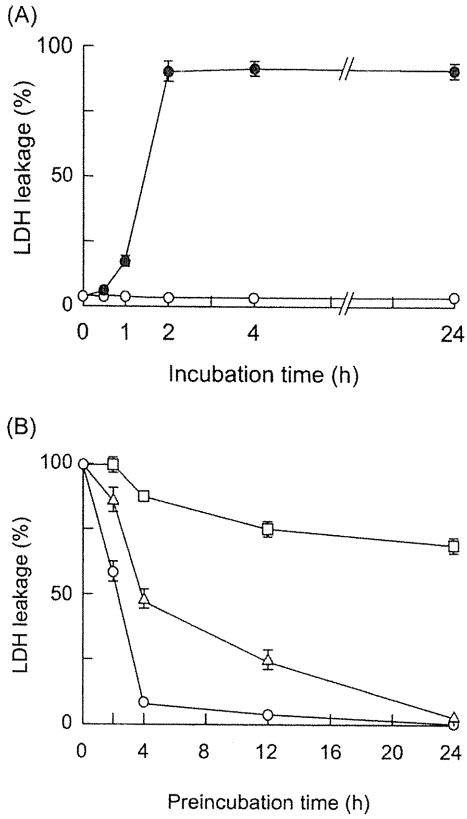

Fig. 3. Time course of CSE-induced LDH leakage (A) and quenching of cytotoxic activity of CSE at varying temperatures (B). A) After C6 glioma cells were incubated with vehicle (open circles) or 5% CSE (closed circles) for the indicated time intervals, LDH activity leaked into culture medium was assayed and represented as a percentage of the total activity in the cells. B) CSE was preincubated at 4°C (open squares), 25°C (open triangles), and 37°C (open circles) for the indicated time intervals (2 – 24 h) in the absence of the cells. The preincubated CSE was added to cultured C6 glioma cells, and 4 h later, LDH leakage from the cells was measured. Data are presented as means ± S.E.M. of the values from three experiments, each in triplicate.

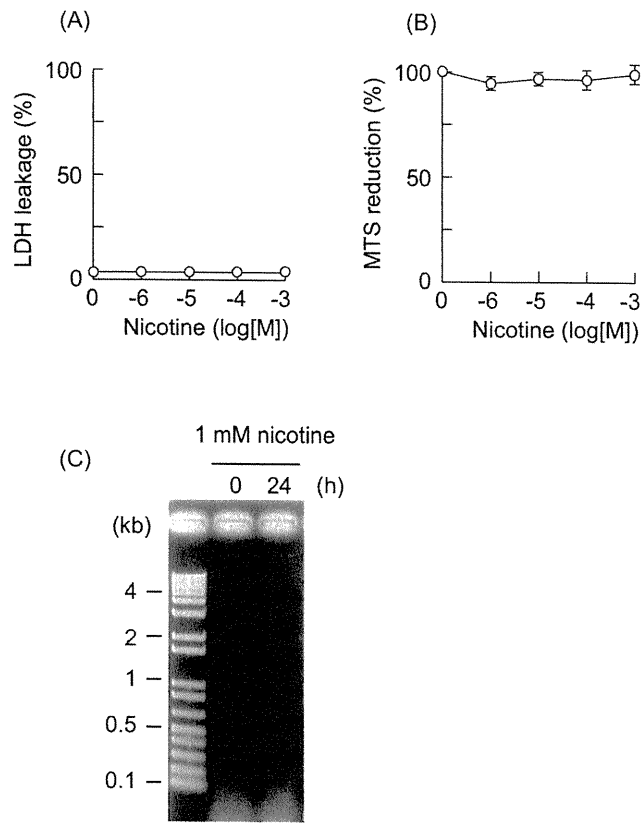

Fig. 4. Effects of nicotine on LDH leakage (A), MTS reduction (B), and DNA fragmentation (C) in C6 glioma cells. After C6 glioma cells were incubated with the indicated concentrations of nicotine either for 4 h with LDH leakage and MTS reduction assays or for 24 h with DNA fragmentation assays on agarose gel electrophoresis; they were subjected to either of the assays as described in Materials and Methods. For LDH leakage and MTS reduction activity, data are presented as means ± S.E.M. of the values from three experiments, each in triplicate.

due to ROS in CSE, which was generated upon burning of tobacco.

Nicotine's effects

To examine whether nicotine is involved in the CSE-induced cytotoxicity or not, we analyzed the effect of nicotine on LDH leakage, MTS reduction activity, and DNA fragmentation in C6 glioma cells (Fig. 4). Nicotine at concentrations up to 1 mM was found to be without effect on LDH leakage (Fig. 4A), MTS reduction activity (Fig. 4B), and DNA fragmentation (Fig. 4C). These results taken together indicate that nicotine is not involved in the cytotoxic activity of CSE.

CSE-induced cell damage is due to apoptosis

As shown in Fig. 5A, when the cells were incubated for 24 h with vehicle alone, the number of the cells positive for TUNEL staining was negligible. In contrast, after incubation with 5% CSE for 24 h, virtually all of the cells were positive for TUNEL staining. Likewise, when the cells were incubated with 5% CSE for 24 h, DNA from the cells showed fragmentation on agarose-gel electrophoresis (Fig. 5B). Furthermore, to visualize changes in the morphology of cell nuclei, the cells treated with CSE for 24 h were fixed, permeabilized with Triton X-100, and stained with PI. Confocal microscopic analysis of the PI-stained cells showed small and pyknotic nuclei typical of cell apoptosis (Supplementary methods and Figure: available in the online version only). These data taken together indicate that the CSE-induced cell damage is due to apoptosis.